Infiltrating CD8+ T cells and M2 macrophages are retained in tumor matrix tracks enriched in low tension fibronectin fibers

Author(s):
Fonta, Charlotte M.; Loustau, Thomas; Li, Chengbei; Surendran, Suchithra Poilil; Hansen, Uwe; Murdamoothoo, Devadarssen; Benn, Mario C.; Velazquez-Quesada, Ines; Carapito, Raphael; Orend, Gertraud; Vogel, Viola

Publication date:
2023-02

Permanent link:
https://doi.org/10.3929/ethz-b-000594873

Originally published in:
Matrix Biology 116, https://doi.org/10.1016/j.matbio.2023.01.002

Funding acknowledgement:
156931 - Mechanotransduction processes, from the cell periphery to the nucleus, in 2D versus 3D microenvironments (SNF)
175839 - Mechanobiology of Extracellular Matrix (SNF)

Infiltrating CD8+ T cells and M2 macrophages are retained in tumor matrix tracks enriched in low tension fibronectin fibers

Charlotte M. Fonta [a], Thomas Loustau [b,d,e], Chengbei Li [b,d,e], Suchithra Poilil Surendran [b,d,e], Uwe Hansen [f], Devadarssen Murdamoothoo [b,c,d,e], Mario C. Benn [a], Ines Velazquez-Quesada [b,c,d,e], Raphael Carapito [d,e,g], Gertraud Orend [b,c,d,e] and Viola Vogel [a]

a - Laboratory of Applied Mechanobiology, Institute of Translational Medicine, Department of Health Sciences and Technology, ETH Zurich, *Vladimir Prelog Weg, Zurich CH-8093, Switzerland*
b - The Tumor Microenvironment Laboratory, INSERM U1109, Hôpital Civil, Institut d' Hématologie et d'Immunologie, *1 Place de l'Hôpital, Strasbourg 67091, France*
c - MN3T (The Microenvironmental Niche in Tumorigenesis and Targeted Therapy), INSERM U1109, *3 avenue Molière, Strasbourg, Hautepierre, France*
d - Université Strasbourg, *Strasbourg 67000, France*
e - Fédération de Médecine Translationnelle de Strasbourg (FMTS), *Strasbourg 67000, France*
f - Institute for Musculoskeletal Medicine (IMM), *University Hospital Muenster, Muenster, Federal Republic of Germany*
g - Platform GENOMAX, INSERM UMR_S 1109, Institut thématique interdisciplinaire (ITI) de Médecine de Précision de Strasbourg, Transplantex NG, Faculté de Médecine, *Fédération Hospitalo-Universitaire OMICARE, LabEx TRANSPLANTEX, Strasbourg 67091, France*

Corresponding author at: *The Tumor Microenvironment laboratory, INSERM U1109 gertraud.orend@inserm.fr*

Corresponding author at: *Laboratory of Applied Mechanobiology, ETH Zurich viola.vogel@hest.ethz.ch*
https://doi.org/10.1016/j.matbio.2023.01.002

Abstract

Tracks rich in matrix and cells, as described in several cancer types, have immunosuppressive functions and separate tumor nests and stroma, yet their origin is unknown. Immunostainings of cryosections from mouse breast tumors show that these tracks are bordered by an endothelial-like basement membrane, filled with fibers of collagen adjacent to tenascin-C (TNC) and low-tension fibronectin (Fn) fibers. While present in early-stage tumors and maturing with time, tracks still form under TNC KO conditions, however, host (not tumor cell)-derived TNC is important for track maturation. Tumor infiltrating leukocytes (mostly M2 macrophages and CD8+ T cells) are retained in tracks of early-stage tumors. Following track maturation, retained tumor infiltrating leukocyte (TIL) numbers get reduced and more CD8+ TIL enter the tumor nests in the absence of TNC. As these tracks are enriched with platelets and fibrinogen and have a demarcating endothelial-like basement membrane often adjacent to endothelial cells, this suggests a role of blood vessels in the formation of these tracks. The Fn fiber tension probe FnBPA5 colocalizes with TNC and immune cells in the tracks and shows decreased binding in tracks lacking TNC. Consequently, FnBPA5 can serve as probe for tumor matrix tracks that have immune suppressive properties.

Introduction

Tracks rich in extracellular matrix (ECM) and diverse cells, also called tumor matrix tracks [1–3], are observed in various tumors [1,2,4,5], yet their morphological origin and functions are still poorly understood. They are rich in tenascin-C (TNC) and other ECM molecules, and were observed in different tumor types including murine oral squamous cell carcinoma (OSCC) [6], murine breast tumors [2,5,7], murine and human primitive neuroectodermal tumors (PNET) [1], as well as in human melanoma [4], insulinoma [1], colorectal carcinoma [1], and head and neck squamous cell carcinoma (HNSCC) [6]. These tracks appear to organize tumors into nests of tumor cells and interdigitating stroma [5–7]. While such tracks were identified in tumors, other matrix-rich structures also containing TNC were described in tumors: tumor-associated collagen signatures 3 (TACS3), that present dense collagen fibers aligned in perpendicular orientation to the tumor nests in breast cancer [8,9], and reticular fibers in the spleen, lymph nodes and thymus coined "conduits" [10–12]. Temporal profiling of the breast tumor microenvironment (PyMT breast cancer model) reveals collagen XII as a critical component that regulates collagen type I organization and thereby creates a permissive microenvironment that facilitates metastasis [13]. The origin of the cancer-associated tracks is still unknown, and different hypotheses were advanced based on their composition, shape and branching patterns, reminiscent of blood or lymphatic vessels. Indeed, while some hypothesize that these structures might be of either angiogenic, lymphangiogenic or thymic origin, the absence of endothelial cells (ECs) in the tracks of some tumors [4] raised the questions whether they might alternatively be non-endothelial cell-lined tubular channels described as vasculogenic mimicry [14,15], or even result from a genetic program encoding reticular fibers in normal tissues [16]. It is also not clear whether these matrix-rich tracks are tumor type specific, or even specific to different tumor locations. Recent work suggesting that these tracks play an active role in immune suppression [5–7], highlights the urgency to learn more about their origin and morphogenesis, especially regarding the reciprocal crosstalk between the track-specific ECM and the cells residing around and within the tracks.

Pathological alterations of the reciprocal cell-ECM crosstalk is pivotal to tumor formation and progression [17]. Gaining insights into ECM remodeling processes in tumorigenesis and understanding how these tracks form is essential to better identify factors driving tumor growth and metastasis, as well as to better elucidate how the composition and morphology of these structures influence tumor immunity. All this information could be highly useful for diagnosis or anti-cancer therapy. These tracks were described to be enriched in ECM such as, collagen IV, collagen V, collagen VI, collagen XII, fibronectin (Fn), thrombospondin 1, laminins (LM) (LMα5, LMγ2, but not LMα1), and TNC [1,4].

TNC and Fn were identified as indicator molecules of an "angiogenic switch" [18], a phenomenon enabling the switch from vascular quiescence to the formation of new blood vessels, termed angiogenesis [19,20]. This angiogenic switch allows the creation of the tumor's vasculature, well connected to the organs' existing hematopoietic and lymphatic vasculature [1,20–22], through which the growing tumor is provided with oxygen and nutrients, but also providing a route for tumor cell dissemination enabling metastasis. Alternatively, the idea that vessel co-option might play a so far neglected role was recently raised, as human tumors typically develop in well-vascularized organs, whereby blood vessels of the normal tissue are used by tumor cells to generate a tumor mass around the vessels [23]. High expression levels of Fn and TNC are characteristic during embryogenesis, tissue growth and wound healing. Whereas Fn fibers are interlaced with other ECM fibers in most adult organs, where they are kept under high tension [24], TNC expression is downregulated and restricted to a few sites such as places of high tension seen in tendons, underneath some epithelia, some stem cell niches and in reticular fibers of lymphoid organs [25]. TNC acts as a damage associated molecular pattern (DAMP) molecule [26] and plays a role in tissue repair, where TNC disappears after resolution of the original insult [25]. However, when TNC expression is not turned off and continues to be highly expressed, as e.g. found in chronic inflammation, fibrosis or cancer, high TNC levels correlate with a stronger pathological phenotype and worsened patient prognosis. TNC was shown to promote many events leading to metastasis [2,25,27]. Organization of TNC in matrix-rich tracks is characteristic of the tumor microenvironment (TME) of many solid tumors [1].

Here we investigated how tumor matrix tracks are formed and what processes drive their morphogenesis. Since it is challenging to probe the morphogenesis of single tracks *in vivo* [28], or to recapitulate them *in vitro*, as there exists no adapted *in vitro* model that can support and, both specifically and adequately, mimic track formation, we took an alternative approach and studied tracks formed *in vivo* in murine breast tumors [2,5]. A special focus on the matrix molecule TNC was chosen as the involvement of tracks in the immune response showed strong dependency on the presence of TNC and on its cellular origin [5,7]. With the same model applied in the current study, it was previously demonstrated that, not only does TNC impact the immune response with TNC-rich tracks retaining macrophages and CD8+ T cells in the stroma *via* a TNC/

CXCL12 complex [6,7], but also, TNC's cellular origin influences the immune response, with tumor cell-derived TNC skewing macrophages towards a M2 pro-tumor phenotype *via* binding of its fibrinogen-like globe domain to toll-like receptor 4 (TLR4) [5,29], hence promoting an immune suppressive TME, tumor growth and metastasis. In a 4NQO-induced oral squamous cell carcinoma (OSCC) model, tracks rich in TNC were also found, again orchestrating an immunosuppressive TME [6]. Moreover, the abundance of matrix and matrix-associated molecules (coined matrisome [30]) was largely reduced in TNC knockout (KO) tumors, suggesting an important role of TNC in regulating matrix expression and assembly, and through that, immune suppression [6]. To ask how TNC influences track formation, as well as the phenotypic differences of matrix structure and architecture in dependence of host- or tumor-derived TNC with time, we took advantage of the murine MMTV-NeuNT and, NT193 breast tumors from a TNC KO or wild type (WT) mouse at an early stage (3 weeks) and end stage (11 weeks) [2]. Transcriptomic gene signatures of these tumors were used to reveal a dependency of the expression of several genes coding for ECM and ECM remodeling molecules, actors of cellular plasticity and the TGF-β signaling pathway, on the high expression of TNC. Notably, in this model it was previously shown that TNC induces epithelial-to-mesenchymal transition (EMT) in the tumor cells *via* the TGF-β signaling pathway [2]. Depending on its cellular source (stromal host or tumor cell), TNC can promote immune surveillance or evasion [5,6], suggesting that the TNC-rich matrix may get remodeled during tumor progression. We describe here that the cellular source of TNC indeed impacts the kinetics of track formation and their spatial organization, and we show for the first time that these tracks, containing an increasing amount of relaxed Fn fibers, mature, and that this has an impact on the abundance of infiltrating macrophages and CD8+ T cells they retain.

Since we initially observed here that the tumor tracks are lined by a basement membrane-like network containing endothelium-expressed laminin α4 (LMα4) [31,32], as well as nidogen and collagen IV, we then asked whether the tracks might have evolved from an endothelium. Since tumor endothelial cells (TEC) have been described to have properties that are different to those of normal ECs, which include a higher proliferation rate leading to multilayered TEC linings, high expression of pro-angiogenic soluble factors and ECM molecules, altogether negatively impacting the function of the tumor blood vessels and tumor immunity [33,34], we further explored whether an endothelial-to-mesenchymal transition (EndoMT) might be involved in the formation of the tumor-associated tracks. In EndoMT, sessile ECs anchored to the basement membrane of vessels get mobilized by fibrotic and tumorigenic factors, and transition towards a migratory mesenchymal cell phenotype [35,36]. EndoMT has been described for endothelia of either blood or lymphatic vessels [37], and can be induced by several pathways including Wnt [27] and Notch signaling [38]. Noticeably, those are two pathways activated by TNC [27]. Other cellular plasticity relevant factors upregulated in the TME include TGF-β, reactive oxidative species (ROS), hypoxia (*via* HIF-1α) and physical factors like elevated ECM stiffness [39].

As TNC is often co-expressed together with Fn in tumors, and since low tension Fn fibers are a hallmark of tumors [24,40], we probed the tensional state of Fn fibers inside the tracks and asked whether it changes during track maturation. We therefore exploited a Cy5-labeled fibronectin binding peptide A5 (FnBPA5) tension probe whose multivalent binding motif to the N-terminal Fn domains FnI_{2-5} is destroyed by stretching Fn fibers [24,40,41]. As the stretching of Fn fibers can modulate the affinity of binding partners and cell fate [42], we finally discuss how the tensional state of Fn fibers within the tracks could modulate the track-associated niche properties for M2 macrophages and CD8+ T cells and propose that the detection of Fn fibers tensional state could serve as novel tool to detect stromal niches with immune suppressive properties.

Results

The track cores contain significant amounts of cellular Fn and TNC, and are surrounded by a shaft of endothelial basement membrane proteins

As the tumor matrix tracks were described as ECM-rich tubular structures [1], we started out by characterizing the ECM composition of tracks by immunofluorescence staining using distinct and validated tumor mouse models in which matrix-rich tracks were previously reported: the MMTV-NeuNT tumors [2] and the syngeneic NT193 grafted breast tumors [2,5] (Supplementary Fig. S1A and B). In the MMTV-NeuNT (NeuNT), the constitutively active form of mutated rat ErbB2 (NeuNT) drives multifocal adenocarcinomas in the mammary gland and metastasis in the lung [2,43–45]. Here, we used tumors from WT and TNC KO mice. The NT193 grafted breast tumor model is a syngeneic orthotopic breast tumor model, where the NT193 tumor cell line was derived from a NeuNT tumor [46]. NT193 cells engineered with a control shRNA (shC) and shRNA to downregulate TNC (shTNC) were grafted into the mammary gland of a WT or TNC KO syngeneic host, respectively, resulting in tumors with either TNC expression from both host and tumor cells

(WT/shC), or in tumors with essentially no TNC expression (KO/shTNC) (Supplementary Fig. S1B). High TNC expression in WT/shC and close to no TNC in the KO/shTNC tumors was previously described [2].

The track characterization was performed on cryosections of tumors extracted 11 weeks after tumor initiation (NT193) and 4−5 months after tumor palpation (NeuNT model), respectively as described in Supplementary Fig. S1A and B. Immunostaining with antibodies for TNC, collagen I, Fn, as well as for eminent basement membrane proteins laminin (pan LM), collagen IV and nidogen confirmed that these tumor tissues are rich in matrix proteins, forming tracks arranged in a dense network that typically extends from the outer shell of the tumor towards the interior (Fig.1A). Zoom-in images of the NeuNT tumor borders clearly depict the tracks connected to the tumor's outside shell, as if they were emerging from the tumor outside shell region, potentially having grown toward the inside of the tumor body, attracted by oxygen or morphogenic gradients (Fig.1A). Our results confirmed that these track structures are rich in TNC (Fig.1B−G), Fn (Fig.1B and D), and collagen I (Fig.1C) [1,2,8]. We also observed, associated with the tracks, matrix molecules that typically are found in the basement membranes, in particular laminin (pan LM) (Fig.1A, D, E), collagen IV (Fig.1F) and nidogen (Fig.1G).

To determine whether the Fn fibrils detected in the tracks, mostly originate from blood-circulating plasma Fn, or from cellular Fn, additional tissue staining was performed with a monoclonal antibody that recognizes the EDA domain of Fn, a marker of cellular Fn [47−49]. Fig. 1D illustrates the high content of Fn-EDA in the tracks, indicating the presence of cellular Fn which could have been produced by cells inside or in close vicinity to the tracks.

To gain insights into the internal architecture and organization of the ECM proteins that define the tracks, line profile plots of track cross-sections were further analyzed. As depicted by the fluorescence intensity peaks of the immunostained markers across the tracks, the TNC signal is closely associated with that of Fn, Fn-EDA and collagen I, which suggests close proximity, or even colocalization of these molecules with TNC in the core of the tracks (Fig. 1B−D). Comparison between the confocal fluorescence images of the tracks and the line profile plots suggests that fluorescence intensity peaks correspond to individual ECM fibers. Thus, the observed highly overlapping fluorescence intensity peaks could originate from TNC proteins that are intertwined with Fn fibers as well as with collagen I fibers. The collagen IV signal was also closely associated with TNC. While TNC fluorescence intensity peaks, characteristic of individual TNC fibers, are mostly concentrated in the core of the tracks, the collagen IV signal displays intensity peaks more towards the rim of the tracks and is reduced in the track core (Fig. 1F). Similarly, LM is mostly localized at the borders of the tracks, and not in the core (Fig. 1D and E). While some nidogen can be found inside the tracks, most nidogen is located at the track borders, as indicated by the high intensity peaks surrounding the TNC peaks in the line profile (Fig. 1G). As basement membrane proteins line the shaft of the tracks, we next asked whether ECs can be detected in association with the tracks by staining for the endothelial cell marker CD31/PECAM1. Representative fluorescence imaging reveals the presence of CD31 positive cells in close association with the tracks (Fig. 1H), as well as enhanced signal surrounding the lumen of the vessels (Fig. 1J).

To better describe the stromal cellular niche inside the tracks and identify whether fibroblasts or myofibroblasts are the primary cells that actively assemble and remodel the ECM in tracks, additional tissue staining was performed. Antibodies against the fibroblastic markers fibroblast-specific protein 1 (FSP-1) and α-smooth muscle actin (α-SMA) were used to detect fibroblasts and myofibroblasts, respectively. Since CD31 positive cells were observed associated with the tracks (Fig. 1H and J), we investigated the presence and properties of TEC in more detail with antibodies against CD31 and vimentin to detect TECs and mesenchymal cells, respectively [36]. While FSP-1 positive cells can be detected in the tracks and their surrounding (Fig. 1I), some α-SMA positive myofibroblasts are also detected, mostly surrounding the tracks, that are enhanced around blood vessels (Fig. 1J). The α-SMA signal around the tracks could indicate the presence of either myofibroblasts, smooth muscle cells surrounding the endothelium, or, pericytes [50] or pericyte-like cells recruited to the tumor vessels [51,52]. The presence of FSP-1 positive cells and α-SMA positive cells agrees with previously reported track compositions in murine Rip1-Tag2 insulinomas, and some human tumors [1], now also observed in the NT193 model.

Tissue staining reveals that matrix tracks share some blood vessel features

To further investigate whether the LM layer at the track border potentially derives from an endothelium, we stained for the endothelial basement membrane marker LMα4 [31,32] and observed that indeed CD31 and LMα4 were juxtaposed confirming an endothelial origin of the basement membrane (Fig. 2A and B). Adjacent to LMα4, we found TNC (Fig. 2A). In some areas, a CD31 signal next to LMα4 and TNC is not detected anymore, indicating that ECs or potentially TECs either have lost their identity (potentially through an EndoMT) or have died (Fig. 2A, green arrow).

To gain more insights into the organization of the tracks, we further investigated the borders between

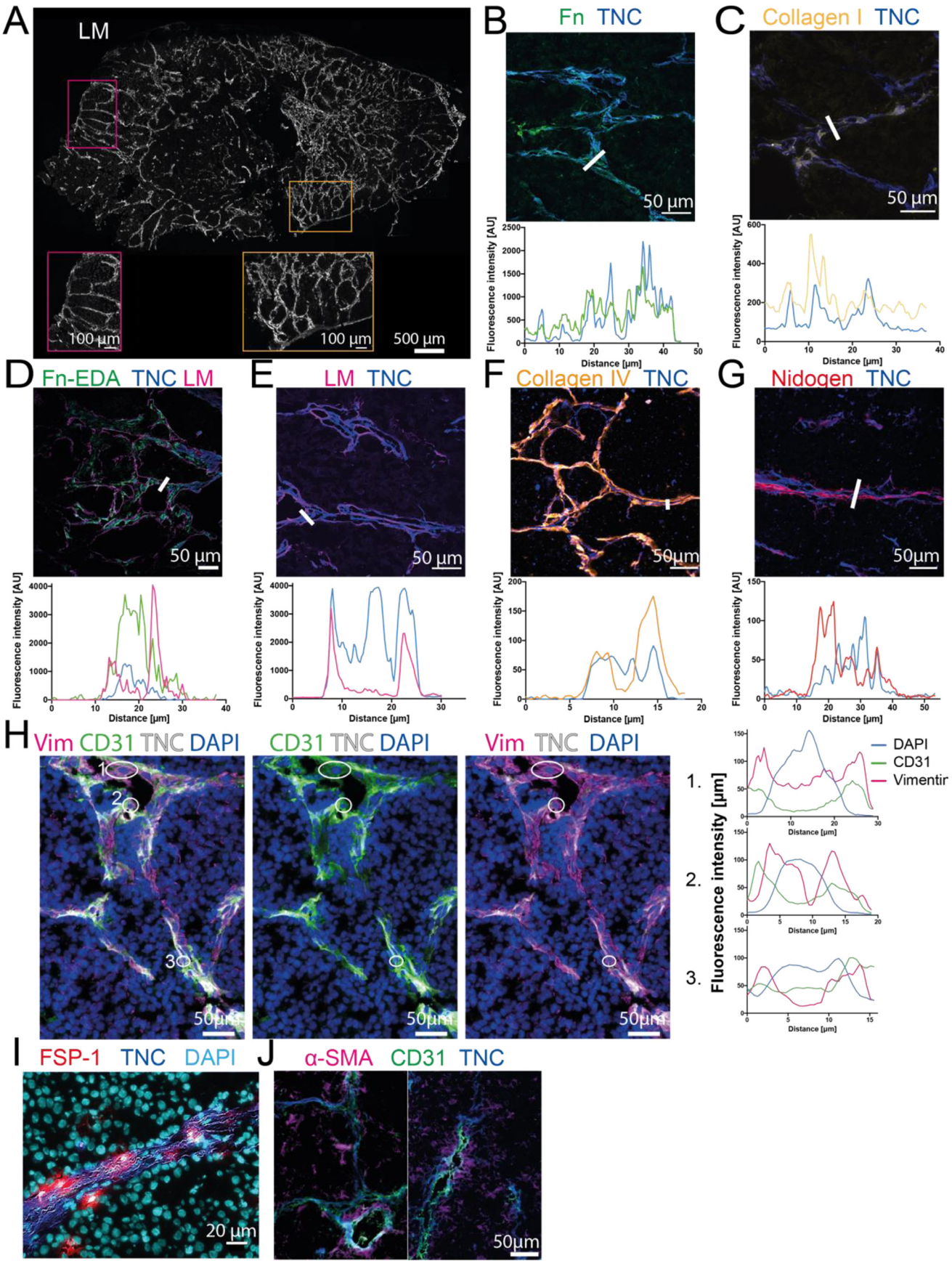

Fig. 1. Track composition and organization in two complementary murine breast tumor models (NT193 and MMTV-NeuNT). A: Overview of a full NeuNT+/+ tumor cryosection displays the network of tracks, detected with a pan LM

the tracks and the adjacent cells of late stage NT193 tumors (WT/shC) by electron microscopy (EM) imaging. We saw a typical dense basement membrane that is lining some areas of the tracks with parallel aligned collagen fibers (stars) confirming lining of the tracks by a basement membrane (Fig. 2C). These high resolution EM images reveal a close apposition of fibrillar collagen fibers to the basement membrane of non-collagenous ECM molecules intermingled with the collagen fibrils (Fig. 2C top panel). The basement membrane has different width depending on the orientation within this 70 nm tissue section. Some parallel aligned collagen fibers are also found to be present between cells where again the basement membrane of Cell number 1 is in contact with the collagen tracks (Fig. 2C bottom panel).

As the endothelium could be part of lymphatic or blood vessels, we stained for platelets (CD41) known to be associated with blood, but not with lymphatic vessels. Indeed, platelets were highly abundant in and around the vessels confirming that the CD31 positive structures are leaky blood vessels (Fig. 2D). Also the staining for fibrinogen (FBG) confirmed that the blood vessels were leaky allowing also FBG to diffuse into the adjacent tissue (Fig. 2E). Collagen XII was previously found to colocalize with TNC in matrix tracks [6]. Moreover, collagen XII binds to collagen I-containing fibrils and is implicated in the regulation of its fibrillogenesis [53]. Staining for collagen XII, revealed a high abundance of collagen XII in the interior of the tracks and in vicinity to CD31 (Fig. 2E). Finally, we stained for the pan leukocyte marker CD45 and noticed a high abundance of tumor infiltrating leukocytes (TIL) associated with ECs/TECs forming cell clusters (Fig. 2F). EC clusters reminiscent of TECs have previously been described in other tumors and are believed to impair blood vessel functions [33,34].

Thus, an endothelium-derived basement membrane surrounds the matrix tracks, bordering ECs/TECs, TNC, collagen XII and the tumor nest. Moreover, highly abundant platelets as well as FBG vessel leakage and EC/TEC cluster formation, suggest that these blood vessels may be poorly functional. The close vicinity of the endothelial basement membrane to track-expressed collagen XII and TNC suggests that the matrix tracks have evolved from blood vessels.

TNC KO does not prevent track formation, but causes differences in track morphology and reduces track density compared to WT tumors

To identify the effects of TNC on track formation and architecture, and to get deeper insights into the mechanism involved, two complementary breast tumor models with engineered TNC levels were studied, the MMTV-NeuNT (NeuNT+/+ expressing TNC and NeuNT -/- KO for TNC) [2] and syngeneic NT193 breast tumors [46] with high (WT/shC) and low TNC (KO/shTNC) [2] (Supplementary Fig. S1A and B).

For both genetic and grafted tumor tissues, tracks are consistently filled with Fn in their cores and LM at the borders (Fig. 3A−D). TNC is detected in the core of TNC-expressing tumors (NeuNT+/+ and WT/shC) (Fig. 3A and C) and is absent from TNC KO tumors (Fig. 3B and D). Interestingly, even in the absence of TNC, tracks form and their composition seems similar, with aligned Fn fibers and LM layers (Fig. 3B and D), suggesting that TNC is not required for tracks to emerge and that high TNC levels do not precede their assembly. Profile plots of Fn, LM and TNC fluorescence intensity across track cross-sections reveal similar track composition and structure for the genetic and grafted TNC-expressing tumors that display an overlap of Fn and TNC signal peaks, evidencing potential colocalization and intertwined Fn and TNC fibers in the track cores (Fig. 3A and C). The LM signal is also conserved between these two TNC-expressing tumors, where intense peaks of LM are observed bordering the TNC peaks, most likely indicating the presence of LM at the borders of the track, surrounding the TNC-rich track core (Fig. 3A and C). Intensity profile plots across tracks in the TNC KO tumors (NeuNT-/- and KO/shTNC) confirm the absence of TNC (Fig. 3B and D). At the here-studied tumor end stage (11 weeks post tumor cell grafting for NT193 tumors and 4−5 months after initial tumor palpation for NeuNT tumors), the MMTV-NeuNT tumors present tracks 1.5-fold wider than the grafted NT193 tumors, while the mean track diameter does not vary between WT and TNC KO tumors of the same tumor model with track diameters of about 22 μm on average in the MMTV-NeuNT tumors and of 15 μm in the NT193 tumors (Fig. 3F). However, Fig. 3B and D depict that the tracks

antibody in tumors, and zoom-in into border areas suggest that the tracks have grown inwards from the tumor border. Scale bar: 500 μm. B-G: Staining of NT193 (WT/shC) tumor cryosections and subsequent line profile plots of track cross-sections reveal a track core rich in Fn (B), TNC (B-G), Fn-EDA (D), collagen I and IV (C, F), that is surrounded by basement membrane proteins LM (D, E), collagen IV (F) and nidogen (G). H: Staining for CD31 and vimentin reveals cells expressing both markers. I-J: FSP-1 positive fibroblasts are also found associated with the tracks and their surrounding (I), and α-SMA-positive cells, that are either smooth muscle cells, myofibroblasts or pericytes, are found surrounding the tracks, enriched in blood vessel areas (J). The image displayed in A was acquired with a slide scanner, images in B-E, J were acquired with a confocal microscope and the images in F, G, H, I were acquired with a brightfield microscope. Scale bars: 50 μm (B-H, J), 20 μm (I). Data shown for 4 sections per tumor. An overview of the mouse models used in this study, and of the associated nomenclature, is given in Supplementary Figure S1.

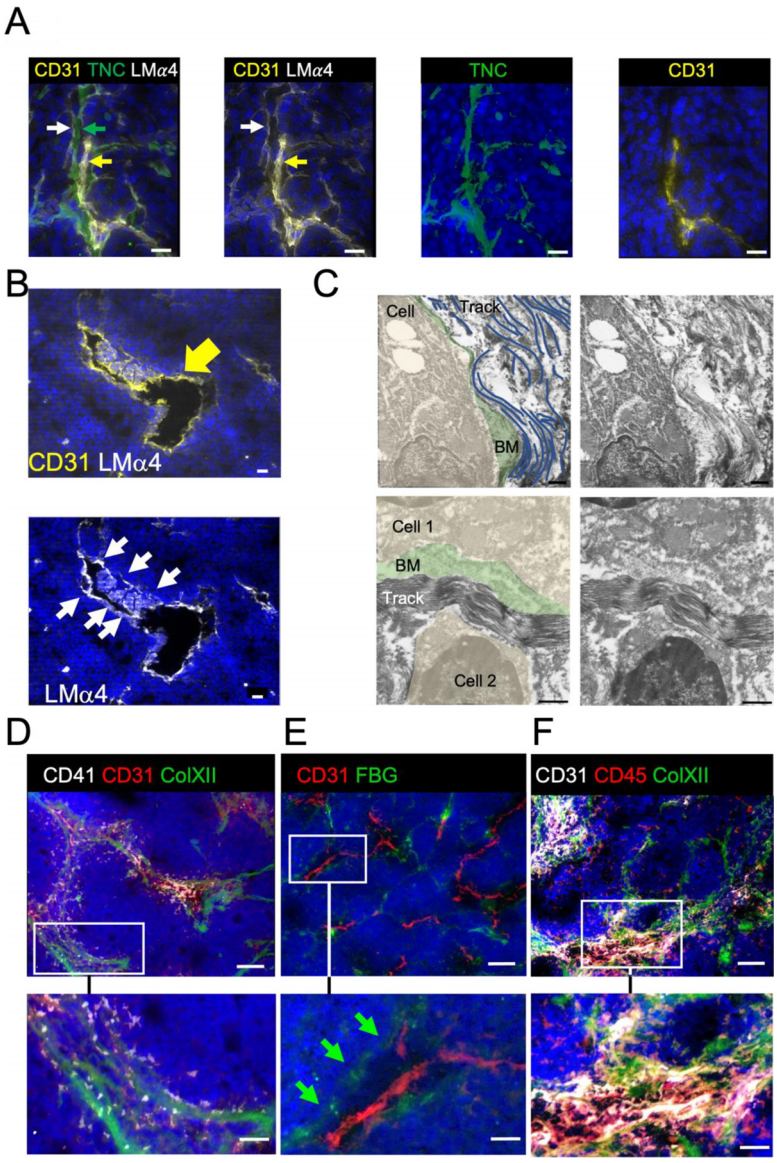

Fig. 2. Blood vessel markers in proximity to matrix tracks in WT/shC tumors as revealed by immunostaining (A, B, D-E) and EM imaging (C). Representative images of 4 distinct tumors and several sections (n = 9) and areas (n = 12) are shown. A: Longitudinal section of a blood vessel reveals juxtaposition of ECs, an endothelial basement membrane and a matrix track. White, yellow and green arrows point at the basement membrane (LMα4), EC (CD31) and TNC (green), respectively. The green arrow points at TNC adjacent to LMα4, but not bordering an EC. B: Sagittal section through a blood vessel that is bordered by a basement membrane (LMα4) and CD31 monolayer and EC/TEC cluster (arrows). **(C)** Electron Microscopy (EM) image revealing a basement membrane (green highlight) separating a cell (brown highlight) from the adjacent matrix track that is filled with parallel aligned collagen fibrils (blue fiber highlight) and other dense ECM material. D – F: Co-immunostaining of CD31 positive vessels with platelets (CD41) and collagen XII (ColXII) **(**D), FBG **(**E) and leukocytes (CD45) and ColXII **(F)**. Note high abundance of platelets around EC/TECs **(D),** FBG localized outside the vessel **(E)** and leukocytes intermingling with clusters of EC/TECs (F). Scale bar, 20 μm **(**A, B**)**, 1 μm (C**)**, 100 μm (zoom-ins of D-F).

appear less organized in the TNC KO conditions, with more track ramifications and nodes (junction of several ramifications).

Here we defined the track density as the percentage of total tissue area covered by ECM tracks. For both the genetic and grafting models, the track density is greater in the TNC WT conditions (NeuNT+/+ and WT/shC) compared to the TNC KO conditions (NeuNT-/- and KO/shTNC) (Fig. 3E). Using zoom-in images of the TNC expressing tumors NeuNT+/+ and WT/shC, we quantified that 8.5% and 6.5% of the total pixels are positive for TNC,

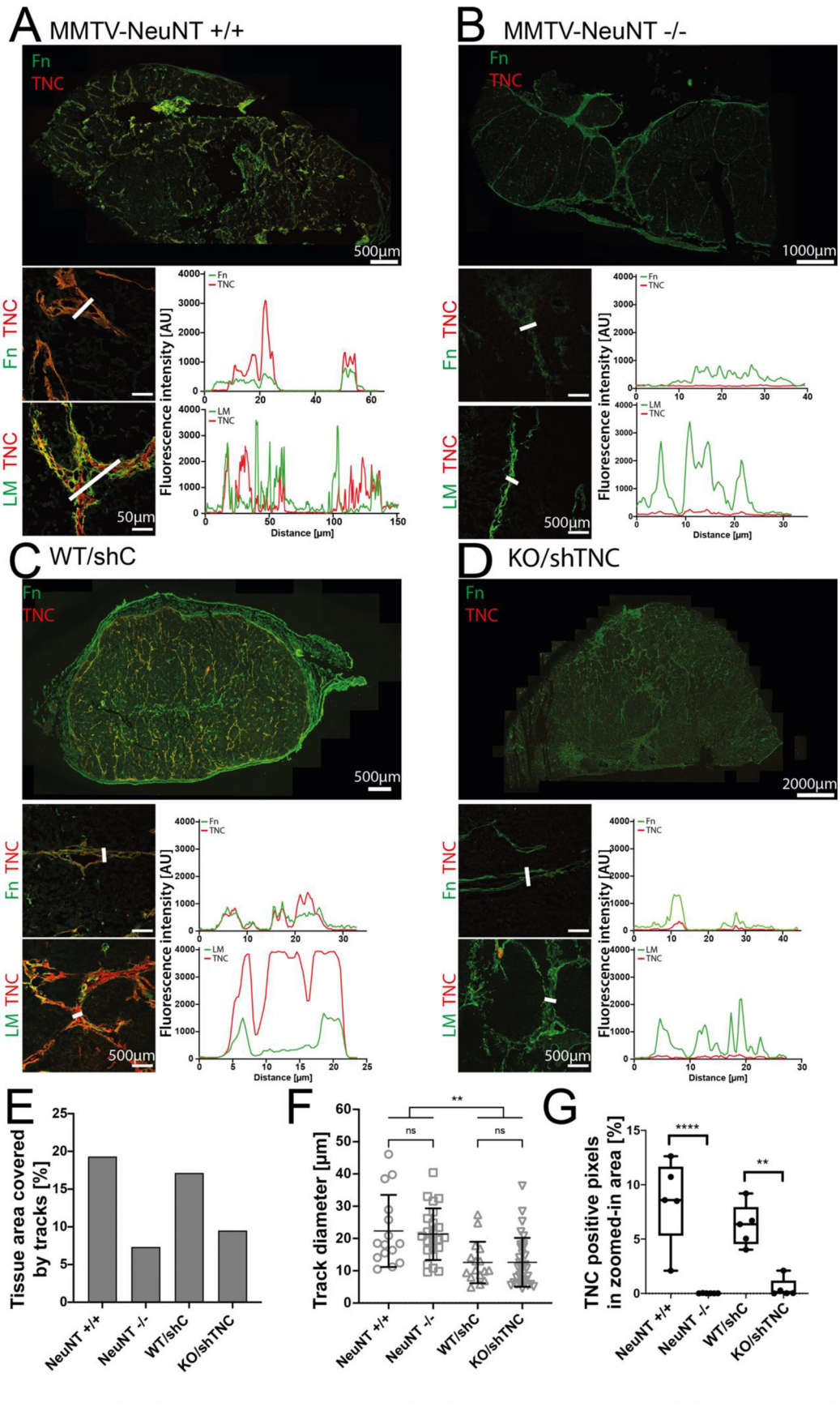

Fig. 3. Tenascin-C (TNC)-expressing tumors display denser and more organized tracks in end-stage tumor cross-sections. A-D: Staining of the genetic MMTV-NeuNT and grafted NT193 tumors, either TNC WT (respectively NeuNT+/+

respectively, while for the TNC KO or knockdown (KD) tumors, TNC expression was at the detection limit with 0% (NeuNT-/-) and 0.2% (KO/shTNC)(Fig. 3G). The non-null detection of TNC in the KO/shTNC tumor tissues can be explained by some residual TNC production by the TNC KD tumor cells (shTNC).

Gene expression data show that TNC expression correlates with higher abundance of ECM remodeling enzymes and of transcription factors participating in cellular plasticity

Since TNC KO tumors showed a decreased density of tracks and a different track architecture (Fig. 3B, D and E), we next asked how the presence of TNC impacts the transcription of genes coding for matrisomal components including ECM, as well as ECM remodeling molecules that could take part in morphological transformations of the tracks. For this purpose, we reanalyzed RNAseq data that had been acquired previously on advanced tumors (11 weeks after tumor initiation for NT193 tumors and 4−5 months after initial palpation for NeuNT tumors as defined in Supplementary Fig. 1A and B [5,7].

Heat maps of whole tissue RNAseq data showcasing low and high gene expression of ECM molecules (Fig. 4A, Supplementary Fig. S2A), ECM remodeling molecules and enzymes (Fig. 4B, Supplementary Fig. S2B), TGF-β signaling pathway members and known inducer of cellular plasticity (EMT and EndoMT) (Fig. 4C, Supplementary Fig. S2C) are given for NeuNT and NT193 tumors with high and no/low TNC, respectively, and show significant differences (minimum fold change 0.8, $p<0.05$). Similarly, anti-adhesive matrix molecules (Supplementary Fig. S2D and E) are also given for NeuNT and NT193 tumors. Expression of several genes encoding for ECM proteins is strongly downregulated in TNC KO conditions such as collagens (collagen I, collagen III, collagen IV, collagen VI and collagen XII), laminins and Fn (Fig. 4A, Supplementary Fig. S2A). Whereas no difference was seen for nidogen at the protein level, as already described at mRNA level (Fig. 4D) thereby confirming previously published data [7], we have seen higher expression of Fn, collagen IV and collagen XII in TNC-rich NT193 tumors by tissue staining and subsequent signal quantification (Fig. 4E−G). Using immunostaining, we observed co-localization of collagen XII with TNC (Fig. 4H). Moreover, as pointed out by the heatmap (Fig. 4A, arrow), in tumors with low TNC, collagen XII is poorly expressed. This has already been noticed in 4NQO-induced tongue tumors [6], and indicates an unknown interdependency of TNC and collagen XII expression also in the here-studied breast cancer model. These results confirm that TNC is an important regulator of the ECM composition in the investigated tumor tissues [6,7]. In TNC KO and KD tumors, genes encoding for major ECM regulators such as the matrix metalloproteinases (MMPs) MMP-1, MMP-2, MMP-3, MMP-8, MMP-9, MMP-11, MMP-13, MMP-14 (also called MT1-MMP), as well as for the ADAM17 protease and for tissue inhibitors of MMPs (TIMPs) TIMP-1, TIMP-2, TIMP-3, TIMP-4 are strongly downregulated (minimum fold change 1.1) (Fig. 4B, Supplementary Fig. S2B). By qRTPCR we confirmed higher levels of *mmps 2, 9* and *14* and a tendency towards higher expression of *mmp3* and *mmp7* in TNC rich tumors, altogether supporting results from the RNA seq analysis (Fig. 4B and I). Lysyl oxidase (LOX) highly expressed in tumors [54,55], and known to promote collagen crosslinking resulting in tissue stiffening [54,56], is downregulated in NeuNT-/- tumors. Similarly, LOXL4 is downregulated in NeuNT-/- and KO/shTNC tumors, hence suggesting that TNC might regulate expression of ECM crosslinking enzymes (Fig. 4B, Supplementary Fig. S2B), beyond its own physical crosslinking activity.

Although the tracks still form even in the absence of TNC in the tumors (Fig. 3B and D), the expression of genes coding for other proteins that modulate ECM synthesis as well as genes coding for essential players of pathways involved in cell and tissue contractility were downregulated in TNC KO tumors. For both TNC KO and KD tumors, the Tgfbr1 gene encoding the TGF-β receptor 1 − TGFβR1 or ALK5

and WT/shC) or TNC KO (respectively, NeuNT-/- and TNCKO/shTNC). Line profile plots of Fn (polyclonal antibody), LM and TNC fluorescence intensities of selected track cross-sections are displayed. A and C: Staining of the TNC-expressing NeuNT+/+ (A) and of NT193 WT/shC tumor (C) cryosections, and associated line profile plots of track cross-sections, reveal a dense network of tracks, rich in Fn and TNC in their core and in LM at the border. B and D: The network of tracks observed in TNC KO conditions in cryosection of NeuNT-/- (B) and of NT193 TNCKO/shTNC (D) is less organized, the tracks contain Fn and LM, but no TNC. E: Track density is greater in TNC-expressing tumors than in TNC KO conditions. F: Despite increased track branching and altered track architecture in TNC KO conditions, track diameter is similar in WT and TNC KO tumor tissues at end-stage tumors (11 weeks after tumor initiation for NT193 and 4-5months after tumor palpation in NeuNT tumors). Tumors of different genetic background though present significant differences in track diameter (One-way ANOVA, $p < 0.01$ (**)). G: Confirming the observed and expected absence of TNC in cryosections of TNC KO tumors (B, D), the percentage of TNC-positive pixels detected in each zoom-in images is greater for WT tumors compared to TNC KO tumors, where no to close to no TNC pixels are detected (One-way ANOVA, $p < 0.01$ (**), $p < 0.001$ (***), $p < 0.0001$ (****)). Scale bars: 500 μm (tumor overview) and 50 μm (zoom-in of tracks). Data shown for 4 sections per tumor.

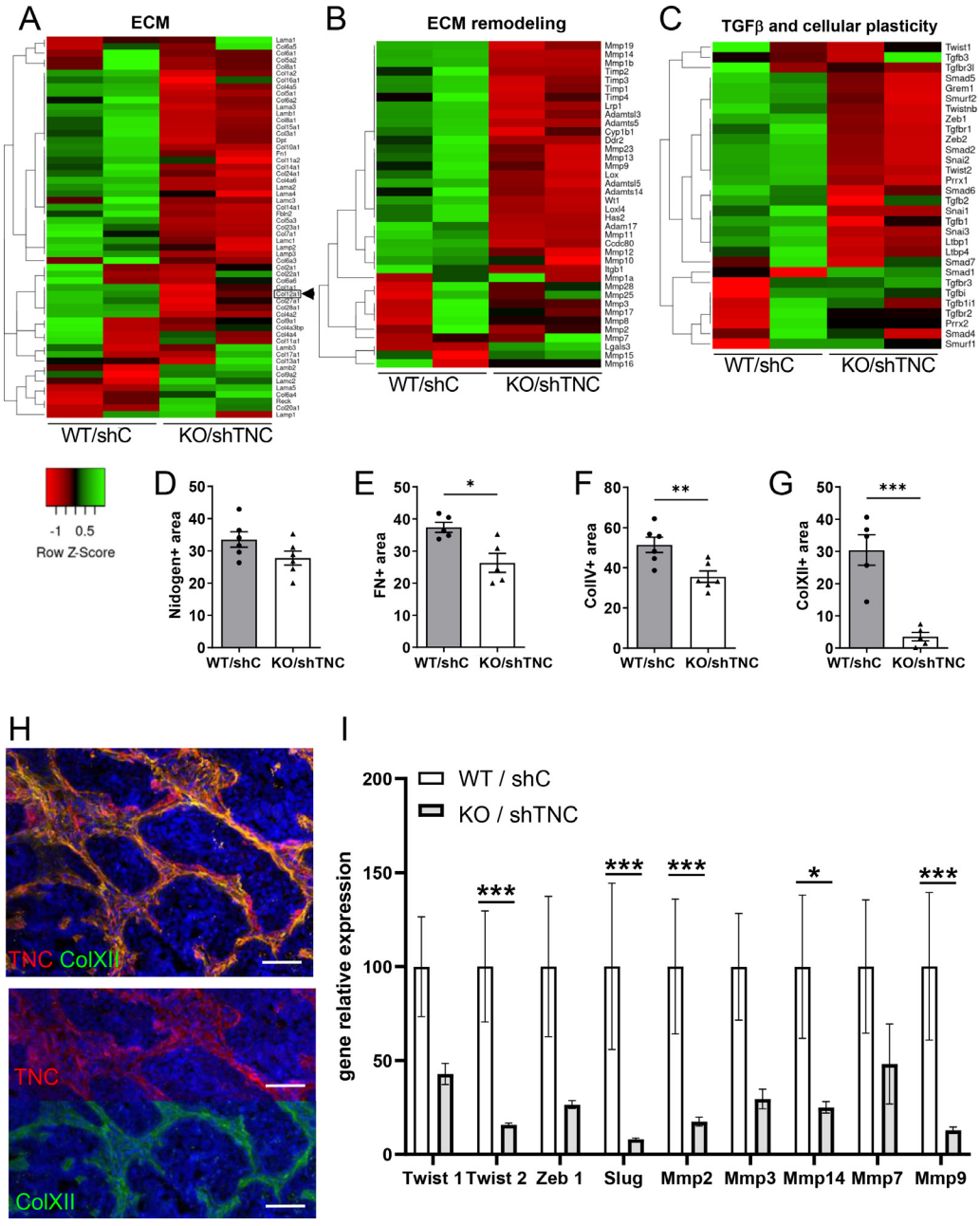

Fig. 4. Tenascin-C (TNC) levels govern expression of genes coding for extracellular matrix (ECM) proteins, ECM remodelers, actors of the TGF-β/Smad pathway, as well as inducers of cellular plasticity. A-C: Heat maps representing the up- (green) and down-regulated (red) genes in TNC-expressing (WT/shC) as well as in KO/shTNC NT193 end stage tumors (n=2). The different heatmaps represent the expression of genes coding for ECM molecules (A), ECM remodeling proteins (B) and actors of TGF-β pathway and cellular plasticity (C). Genes with a minimal fold-change of 0.8 and an adjusted P-value cutoff of 10% are shown. D-G: Quantification of ECM expression, nidogen (D), FN (E), ColIV (F) and ColXII **(G)** on sections (n=6 for Nidogen, Col IV; n=5 for FN, Col XII) from WT/shC and KO/shTNC tumors. One dot represents one tumor. The stained area was determined by Image J as percentage of the total arbitrarily chosen area (Mann Whitney test, *$p < 0.05$, **$p < 0.01$, ***$p < 0.005$, ns $p > 0.05$). H: Representative image (n=3 tumors) of a co-staining experiment for TNC and ColXII of a WT/shC end stage tumor. Note signal overlap. Scale bar: 20 μm. I: Relative expression (%) of the indicated genes in WT/shC (n = 3 tumors, in duplicates) and KO/shTNC (n = 7, in duplicates) end stage tumors as determined by qRTPCR with GAPDH used for normalization. *$p < 0.05$, , *** $p < 0.005$, Mann Whitney test.

− and the Tgfbr2 gene, encoding the TGF-β receptor 2 (TGFβR2) are significantly downregulated compared to the WT tumors (Fig. 4C, Supplementary Fig. S2C). These two receptors are essential for TGF-β signaling that can induce ECM protein expression *via* the TGF-β/Smad pathway [57]. In TNC KO/KD tumors, also TGF-β1, latent TGF-β binding protein (LTBP), smad2 and smad4 are downregulated (Fig. 4C, Supplementary Fig. S2C), altogether revealing a strong impact of TNC on the TGF-β signaling pathway at several levels. This pathway is essential for ECM synthesis in wound healing, fibrosis and tumorigenesis [58,59].

Tumor cell plasticity was shown to be induced by TNC through TGF-β signaling in the NT193 model [2]. Cellular plasticity is also important in EndoMT. However, EndoMT is impossible to assess without lineage tracing *in vivo*. Nevertheless, we looked for indications that cellular plasticity, potentially impacting ECs/TECs, is involved in track formation. Indeed, RNAseq data reveal that the expression of genes coding for EndoMT/EMT factors is correlated with TNC expression. The genes coding for the known EndoMT/EMT inducers Snail-1 and Snail-2, as well as those encoding Zeb-1, Zeb-2, Twist1 and Twist2 [36,60,61] are downregulated in TNC KO/KD tumor conditions (Fig. 4C, Supplementary Fig. 2C). As determined by qRTPCR, *slug* and *twist 2* were significantly higher in WT/shC than in KO/shTNC tumors. A similar trend was also observed for *twist 1* and *zeb1* (Fig. 4I).

The anti-adhesive properties of TNC together with the enhanced detection of TNC in the core of the tracks in WT tumors suggest that the inside of the tracks could present a rather anti-adhesive microenvironment. To further corroborate this possibility, we looked for other adhesion modulatory ECM molecules in tumors with high and low TNC. We observed that Thbs1 encoding thrombospondin-1 (Tsp1) is present inside the tracks of PNET insulinomas [1], as well as Thbs2 and Thbs4, encoding thrombospondin-2 and -4 respectively [62], were downregulated in both breast tumors with no/low TNC (Supplementary Fig. S2D−E). Similarly, also other anti-adhesive molecules of the ECM [63,64], such as tenascin-R (NeuNT tumors), and tenascin-N (both NeuNT and NT193 tumors) are downregulated in TNC KO tumors (Supplementary Fig. S2D−E). In contrast, whereas Sparc itself was downregulated in NT193 tumors, some Sparc family members were elevated (minimum fold change 0.8) in the TNC KO tumors (Spock3 for NeuNT -/- and Spock2, Sparcl1 and Smoc2 for NT193 KO/shTNC), indicating potential maintenance of some anti-adhesive properties in the absence of TNC. Note though that these whole tissue RNAseq data do not permit to specifically locate these anti-adhesive proteins to the tracks.

Fn fibers in the track cores are predominantly in a relaxed tensional state, correlating with high TNC levels

Since TNC KO downregulates transcription levels of molecules involved in ECM mechanobiology regulation and ECM remodeling, such as many MMPs and TIMPs (Fig. 4), we asked whether, and to what extent, the presence of TNC might impact the tensional state of Fn fibers in and surrounding the tracks. Relaxed Fn fibers were indeed previously described as a hallmark of the tumor stroma in contrast to healthy organ tissues [24]. Utilizing the Cy5-FnBPA5 tension probe that binds with high affinity to structurally relaxed Fn fibers in *ex vivo* tissue sections and *in vivo* [24,40], as Fn fiber stretching destroys its multivalent binding, we probed the Fn fiber tensional state in cryosections of both the genetic MMTV-NeuNT and grafted NT193 tumors, either WT (respectively NeuNT+/+ and WT/shC) or TNC KO or KD (respectively NeuNT-/- and KO/shTNC) (Supplementary Fig. 1A and B). The samples were co-stained with antibodies specific for Fn, TNC and LM. Binding of the Cy5-FnBPA5 tension probe is here exclusively detected in tumor tissues (Fig. 5A−D) and not in healthy control tissues (Fig. 5E), where neither TNC, nor matrix tracks were detected. These observations are in accordance with our previous reports identifying Cy5-FnBPA5 binding in tumor but not normal tissues [24,40]. Importantly, zoom-in images of tracks show enhanced binding of the tension probe Cy5-FnBPA5 inside the tracks, as confirmed by fluorescence intensity profile plots of track cross-sections, where the Cy5-FnBPA5 intensity peaks are highly associated with TNC peaks. We thus discovered here an increased presence of structurally relaxed Fn fibers inside these cancer-associated tracks, which are in close proximity to TNC (Fig. 5A−D). Similar to what was shown in Fig. 1E, LM peaks on the line profile plots can be observed at the rim of the tracks, both in presence and absence of TNC however not overlapping with Cy5-FnBPA5 (Fig. 5A−D).

Quantitative analysis of the Cy5-FnBPA5 in tracks shown in Fig. 5F reveals a higher density of Cy5-FnBPA5 in the tracks in the two tumors with high TNC (NeuNT+/+ and NT193 WT/shC) in comparison to tumors with low/no TNC, (NeuNT-/- and NT193 KO/shTNC) (Fig. 5C and D). The Cy5-FnBPA5 pixel density in ECM tracks is here expressed as the percentage of pixels in the tracks that are Cy5-FnBPA5 positive and above a defined threshold. In order to further assess the colocalization of TNC and structurally relaxed Fn fibers in the ECM tracks, both a colocalization and proximity analysis were performed on zoom-in confocal images of the tumor cryosections. For both WT tumor models, in average between 70% and 80% of

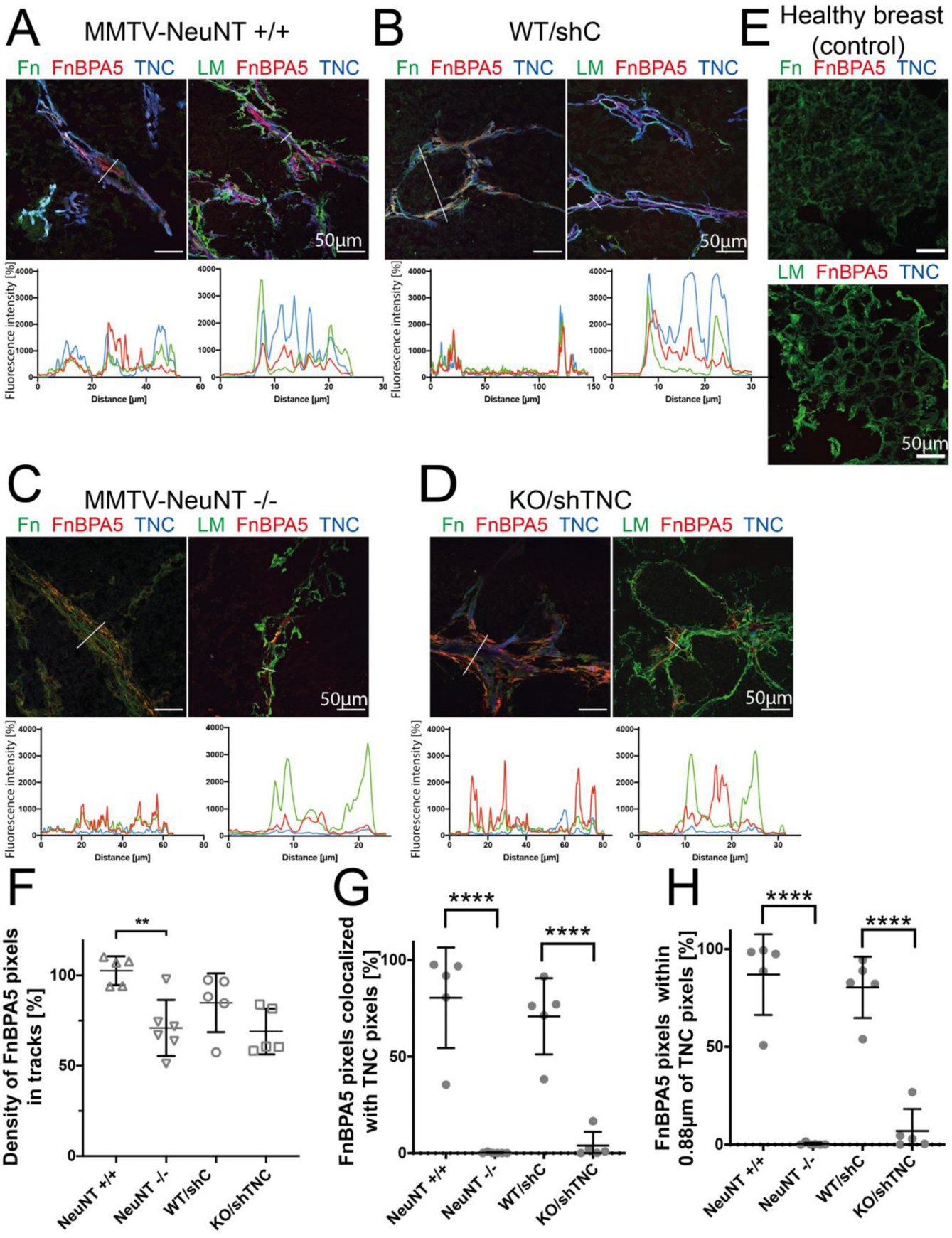

Fig. 5. Fibronectin (Fn) fibers in the tracks are predominantly in a structurally relaxed tensional state and correlate with tenascin-C (TNC) levels. Cy5-FnBPA5 staining coupled with staining of tumor cryosections for Fn, LM and TNC and subsequent line

the TNC pixels in the tracks are colocalized with Cy5-FnBPA5 pixels (Fig. 5G). Similarly, the proximity analysis (studying the 3-by-3 pixels matrix surrounding each TNC positive pixel for the presence of Cy5-FnBPA5 positive pixels), reveals that 86% and 80% of all the Cy5-FnBPA5 positive pixels are within 0.88 μm apart from TNC positive pixels in the NeuNT +/+ and NT193 WT/shC tumors respectively. Essentially no Cy5-FnBPA5 positive pixels can be detected in the 3-by-3 matrix surrounding each TNC pixel in the TNC KO NeuNT-/- and NT193 KO/shTNC tumors as only residual TNC is expressed in these TNC KO tumors. The discovery that Cy5-FnBPA5 binds in tracks and that this binding is proportional to the track density (Figs. 3E and 5F) is of significant interest for two reasons. First, these data illustrate that Cy5-FnBPA5 can be exploited to visualize tumor-associated tracks. Second, this might be functionally highly relevant as relaxed and stretched Fn fibers can display different sets of molecular bindings sites, some being activated others destroyed by fiber stretching [42].

The cellular source of TNC impacts the evolution of track morphogenesis

To gain insight into the morphogenesis of these tumor matrix tracks and whether and how it is impacted by the cellular source of TNC, track composition and organization between early (3 weeks after engraftment) and end stage tumors (11 weeks after engraftment) was studied and compared using the NT193 model, between tumors in which TNC is solely expressed by host stromal cells (WT/shTNC) and tumors in which the TNC is expressed by tumor cells only (KO/shC) (Supplementary Fig. S1C).

Staining of tumor cryosections for the ECM markers TNC, Fn, LM, coupled with Cy5-FnBPA5 staining, and with second harmonic generation (SHG), which permits label-free visualization of dense bundles of thick collagen I fibers [65,66], revealed that, regardless of TNC cellular origin, tracks form in early stage tumors already (Fig. 6B and C, Supplementary Fig. S3A and D).

First, at both early and late time points and regardless of the cellular source of TNC, the distribution of the TNC and Cy5-FnBPA5 signal intensity peaks in comparison to the SHG signal in the line profile plots, strongly suggest that both TNC and structurally relaxed Fn fibers, to which Cy5-FnBPA5 binds, are colocalized with collagen fibers (Fig. 6A−D).

At early tumor stage, tumors are rich in tracks (Fig. 6F). However, while WT/shTNC tumors (host TNC) are rich in TNC, relaxed Fn fibers and present a high parallel and aligned collagen bundle content in their track cores (Fig. 6B and F−G), a different situation can be observed in KO/shC tumors, where the sole TNC source comes from the tumor cells, where TNC and Cy5-FnBPA5 densities in the tissue are lower than in WT/shTNC tumors (Fig. 6F), and the percentage of SHG positive pixels in the track core is lower as well (Fig. 6G). Additionally, at this 3-weeks early time point, KO/shC tumors display multiple, highly unorganized matrix structures with multiple branching points (Fig. 6C, Supplementary Fig. S3C), clearly different in width and organization to the tracks of WT/shC tumors (Fig. 3C) and WT/shTNC tumors (Fig. 6B). Indeed, with a diameter of about 13 μm, the tracks in KO/shC are thinner than in the WT/shTNC tumors at the same (early) tumor stage (20 μm) (Fig. 6H), and also thinner than tracks of WT/shC tumors at 3 weeks (20 μm) (Fig. 6C). Taken together, these observations suggest that stromal cells produce TNC more abundantly than tumor cells in early-stage tumors and that TNC from tumor cells is not necessary, neither for track formation, nor initiation, as there is no visible negative impact on track formation caused by the lack of TNC expression by the tumor cells at this early stage (Fig. 6B, Supplementary Fig.S3A).

In end stage tumors, tracks can still be observed in both WT/shTNC and KO/shC tumors (Fig. 6D and E) with similar densities as in early stages tumors (Fig. 6F). However, for the end stage WT/shTNC tumors, while densities of both TNC and Cy5-FnBPA5 are decreased as compared to the 3 weeks tumors (Fig. 6D and F, Supplementary Fig. S3B), the SHG signals inside the tracks (as depicted by the percentage of SHG pixels), which was already high in the early stage tumors (Fig. 6G) indicating the existence of thick collagen fiber bundles at 3 weeks, shows to still increase in end stage tumors (Fig. 6G). Track diameter in these end stage tumors significantly decreases and narrows down to about 8 μm (Fig. 6H). These observations altogether illustrate major ECM remodeling of the tracks with time. Interestingly, the decrease in track diameter observed in WT/shTNC tumors between early and

profile plots of track cross-sections display enhanced Cy5-FnBPA5 binding inside the tracks of TNC-expressing MMTV-NeuNT +/+ (A) and NT193 WT/shC tumors (B). Decreased Cy5-FnBPA5 binding is observed in MMTV-NeuNT -/- (C) and NT193 KO/shTNC tumors (D), while there are even no Cy5-FnBPA5, no TNC and no tracks in a healthy breast tissue control (E). Similarly, Cy5-FnBPA5 pixel density in ECM tracks is higher for both TNC-expressing tumors as compared to TNC KO/KD tumors (F). Strong colocalization (G) and proximity (H) for the Cy5-FnBPA5 pixels and TNC pixels in TNC-expressing tumors (NeuNT+/+ and WT/shC) (One-way ANOVA, $p < 0.01$ (**), $p < 0.001$ (***), $p < 0.0001$ (****)). Scale bars: 50 μm. Data shown for 4 sections per tumor, one dot is one representative area of the section.

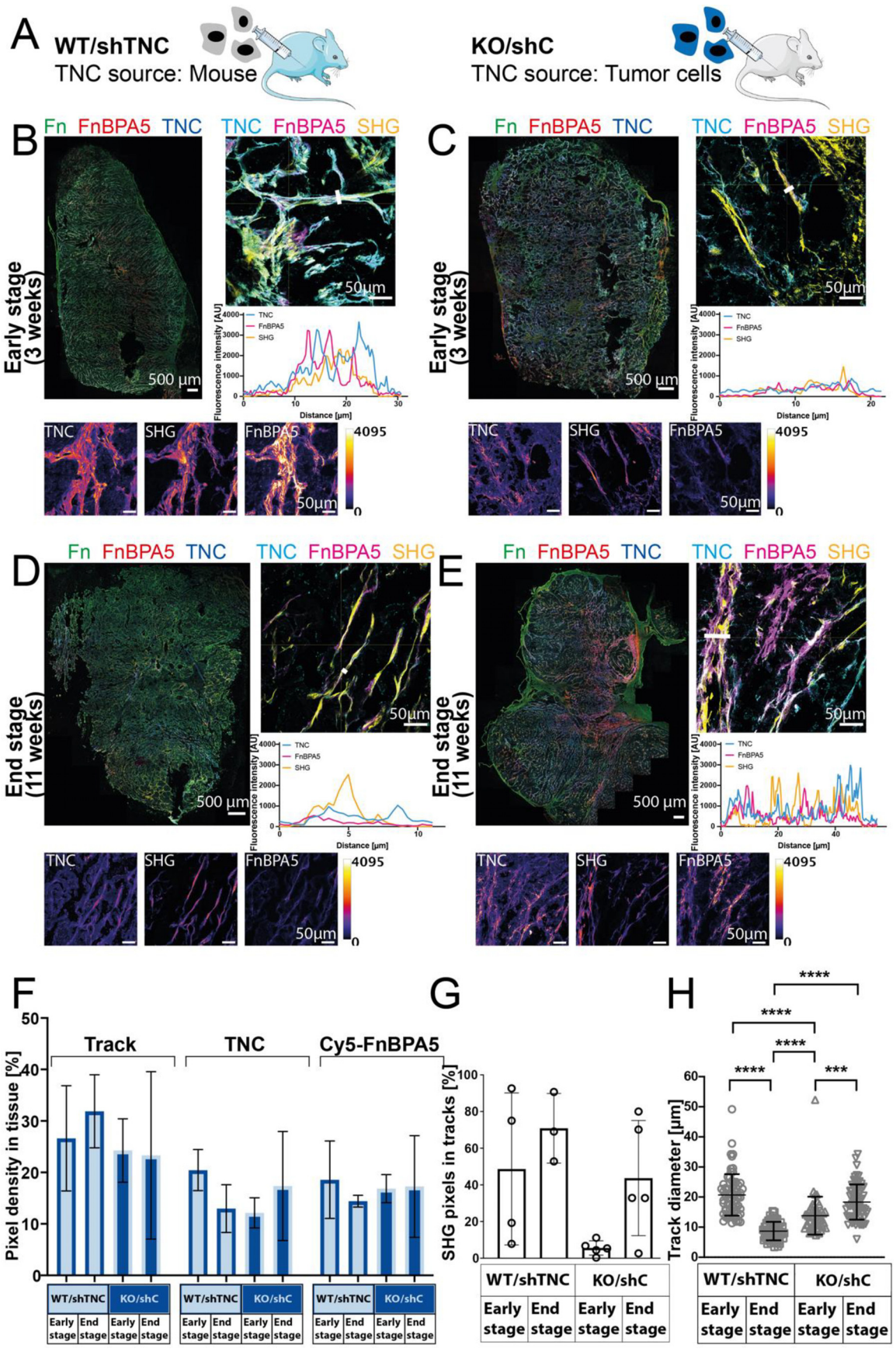

Fig. 6. The cellular source of TNC, either from the tumor or stromal cells, tunes track composition and morphogenesis. A: Description of the WT/shTNC and KO/shC mouse tumor models with, respectively, a stromal versus tumoral cellular

end tumor stages is similar to that observed in WT/shC tumors, where TNC is expressed by both stromal and tumor cells (Fig. 8C), hence hinting a more important role played by stromal cells and TNC expressed by the stromal cells in track formation and structural evolution in time. Here, it should be taken into account that tumor cells express much less TNC than stromal cells [2].

In end stage KO/shC tumors, however, not only is the track diameter increasing (about 18 μm), close to the 20 μm-wide tracks observed in the early stage WT/shTNC tumors (Fig. 6H), but also more organized tracks are observed (Fig. 6E, Supplementary Fig. S3D), richer in dense collagen I bundles (Fig. 6G), in TNC and in structurally relaxed Fn fibers than at early stage, with densities similar to that observed in early stage WT/shTNC tumors (Fig. 6E and F). These results altogether are reminiscent of a delayed maturation of the tracks if TNC is expressed by the tumor cells only or is missing altogether.

Gene expression analysis supports an impact of TNC on blood vessel formation and matrix track maturation

Having established a link between blood vessels and matrix tracks, we addressed which molecules may regulate matrix track maturation by comparing the angiogenesis, matrisome and ECM remodeling gene expression signatures between 3 and 11 weeks of the different NT193 tumors. The heatmap representation clearly shows differences in WT/shC compared to KO/shTNC tumors between 3 and 11 weeks for each tumor (Fig. 7A and B, Supplementary Fig. S4A−F). At 3 weeks, most angiogenesis-associated genes are more expressed in the WT/shC than in KO/shTNC tumors. This seems to change at 11 weeks, when more angiogenesis associated genes are upregulated in KO/shTNC compared to WT/shC tumors. Genes encoding molecules involved in TGFβ signaling such as Tgfb1 and Ltbp2 are upregulated at 11 weeks compared to 3 weeks in the KO/shTNC tumors indicating a potential role in angiogenesis independent of TNC. Altogether, these results indicate that, at 3 weeks, more blood vessels are formed in WT/shC than KO/shTNC tumors with a delay in angiogenesis in the KO/shTNC tumors (Supplementary Fig. S4A−D). A similar scenario is also observed for matrisome-associated genes that are less expressed in WT/shC tumors at 11 weeks than at 3 weeks. This is different in KO/shTNC tumors, where several matrisome genes are more expressed at 11 weeks than at 3 weeks. This shift in gene expression may reflect the observed delay in track maturation in the KO/shTNC tumors (Fig. 7A−D). As the basement membrane stabilizing molecule PRELP (Proline aRginine-rich End Leucine-rich Protein) is more expressed in 11 than 3 weeks WT/shC tumors we ask whether PRELP may play a role in track maturation [67]. A more detailed analysis of the specific roles of the differentially expressed genes could provide insights into candidate molecules driving track maturation for future investigations that is beyond the scope of this article. This comparison also revealed that the majority of genes is not only highly expressed in the angiogenesis signature of WT/shC tumors, but also in the matrisome and ECM remodeling signatures which could further support a potential interconnection between blood vessel remodeling and matrix track formation.

Retention of CD8+ T cells and M2 macrophages inside the tumor tracks evolves with time and track maturation

As TNC was previously shown to retain macrophages and CD8+ T cells in the stroma [5,7], here we compared the presence and localization of tumor infiltrating leukocytes (CD8+ T cells, activated macrophages (F4/80) and M2-polarized macrophages (CD206)) in WT/shC tumors between early (3

source of TNC. B-C: 3 weeks after tumor cells engraftment, tracks can be observed in both tumor models, although more organized in the WT/shTNC (B) as compared to KO/shC tumors (C). Maximal intensity z-projections of stack confocal images show tracks with strong SHG signal for both tumors, but stronger TNC and Cy5-FnBPA5 signals in the WT/shTNC tumors with stroma-derived TNC (B), while very little TNC and Cy5-FnBPA5 are detected in the TNCKO/shC tumors, where TNC is expressed by the tumor cells (C). Additional "temperature" representation of selected tracks, displaying, for each channel, higher intensity pixels lighter and lower intensity pixels darker, confirms the observed lower Cy5-FnBPA5 and TNC signals in KO/shC (C) as compared to WT/shTNC tumors (B). D-E: Similarly, in end stage tumors (11 weeks), both tumor conditions display dense networks of tracks, with higher track organization in the KO/shC tumors (E) as compared to the WT/shTNC tumors (D). While SHG signal indicates the presence of dense collagen bundles in both tumors, the Cy5-FnBPA5 and TNC signals are now lower for WT/shTNC (D) and increased for KO/shC (E). B-E: The line profile plots, with signals of Cy5-FnBPA5 and TNC surrounding the peaks of SHG signals, strongly suggest that TNC and structurally relaxed Fn fibers are assembled into intertwined or even common fibers. F: Comparison of the track density, Cy5-FnBPA5 density and TNC density between the two tumor models, at the two study time points. G: Density of SHG pixels in the tracks increases with time for both tumors, although more for the WT/shTNC tumors as compared to KO/shC tumors. H: Track diameter decreases with time for WT/shTNC tumors, while it increases with time for KO/shC tumors. (One-way ANOVA, $p < 0.0005$ (***), $p < 0.0001$ (****)). Scale bars: 500 μm for full tissue and 50 μm for zoom-in images. N=2 tumors per condition.

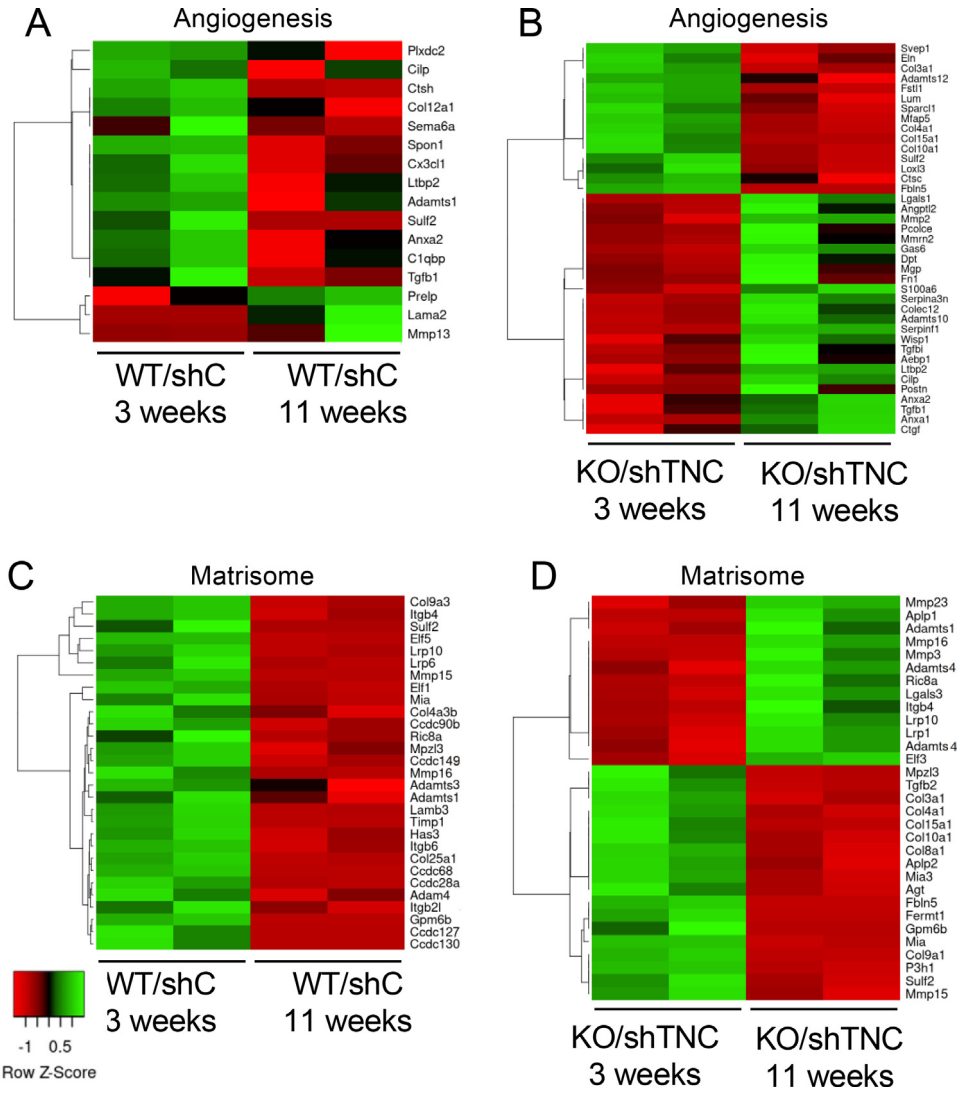

Fig. 7. Tenascin-C (TNC) levels influence expression of angiogenesis and matrisome signatures in NT193 tumors. A-B: Heat maps representing the up- (green) and down-regulated (red) genes encoding for angiogenesis (A, B) and matrisome associated proteins (C, D), by comparing 3 and 11 weeks tumors with high TNC levels (WT/shC) (A, C) and low TNC levels (B, D). Genes with a minimal fold-change of 0.8 and an adjusted P-value cutoff of 10% are shown.

weeks) and end stage (11 weeks), using tissue staining with antibodies against CD8+ cells, F4/80+ cells and CD206+ cells, together with the Fn fiber tension probe Cy5-FnBPA5 (experimental description depicted in Supplementary Fig. S1D). This analysis revealed that CD8+ T cells (around 90% of total CD8+ cells) (Fig. 8J), F4/80+ macrophages (90% of total F4/80+ macrophages) (Fig. 8E) and CD206+ macrophages (70% of total CD206+ macrophages) (Fig. 8G) were highly abundant in the tracks at 3 weeks and less numerous in the end stage tumors (Fig. 8A, B, D, E, G and J, Supplementary Figs. S5 and S6). Similar to previous observations in WT/shTNC tumors (Fig. 6H), we found a track thinning in these WT/shC end stage tumors (Fig. 8C). Additionally, track maturation seemed to be accompanied by a reduced number of cells in the tracks (Fig. 8D). Whereas the total number of CD8+ T cells and F4/80+ macrophages in the tracks decreased in the end stage tumors, this was not seen for CD206+ M2 macrophages (Fig. 8E, G and I). Furthermore, the decrease of F4/80+ macrophages in the tracks is not associated with an increase of these cells in the tumor nests, as indicated by the very low percentage of these cells located in the tumor nests at both early and late stages, hence strongly hinting that the decrease of F4/80+ macrophages in the tracks is not caused by enhanced infiltrations of these cells into the tumor nests (Fig. 8E and F).

Also CD8+ T cell numbers drop in the end stage compared to 3 weeks tumors, namely by over six

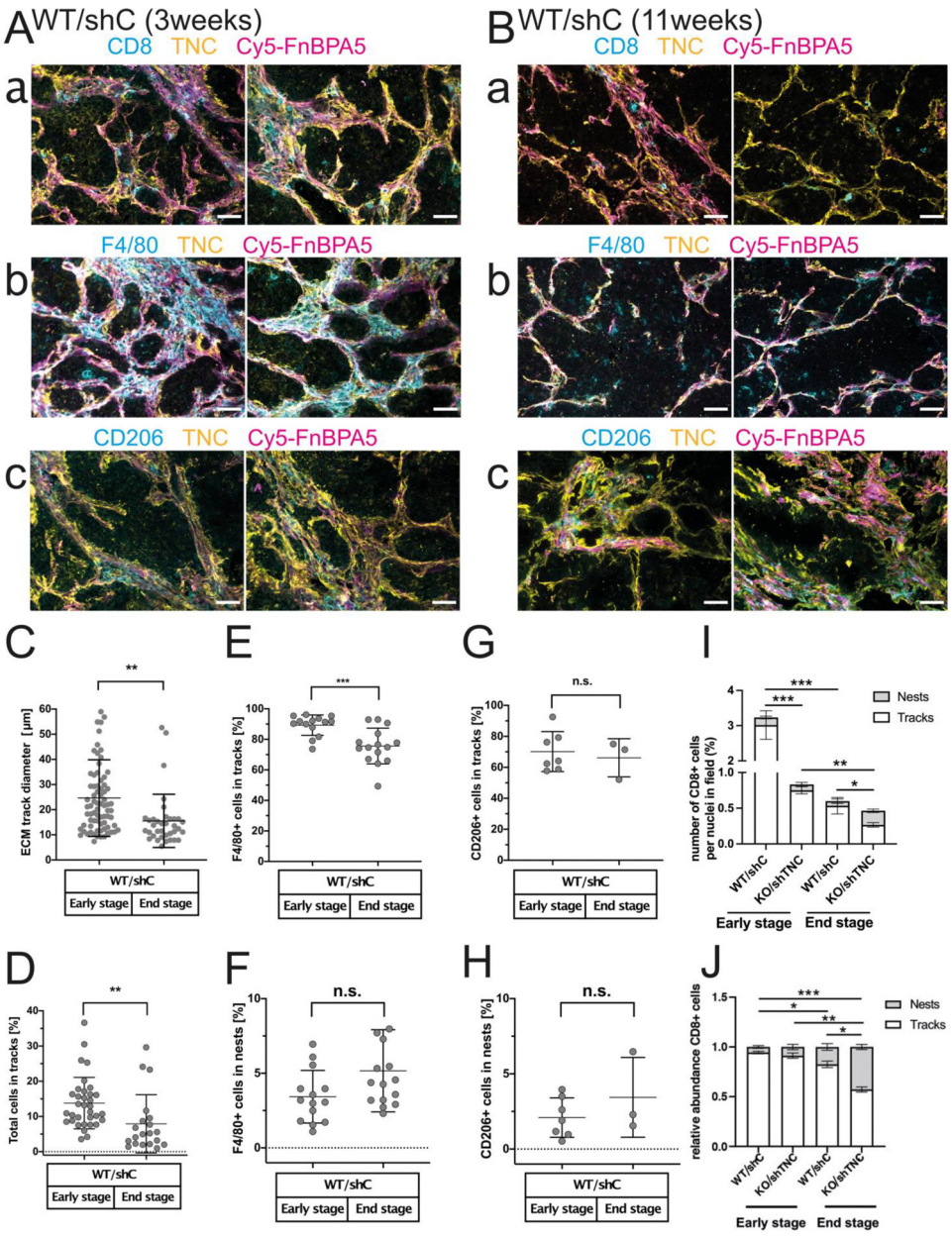

Fig. 8. Enhanced immune cell retention in the tracks in WT tumors (WT/shC) at early stage, decreasing in end stage tumors correlating with changes in track diameter. A-B: Cy5-FnBPA5 stain (magenta) and staining of WT/shC tumors at early and end stage with antibodies against TNC (yellow) and, either, CD8+ T cells (cyan, **a**), F4/80+ macrophages (cyan, **b**) or CD206+ M2-polarized macrophages (cyan, **c**). Scale bars: 50 µm. C: Track width is significantly higher at early stage than in end stage WT/shC tumors. N=3 tumors per conditions, student t-test, $^{**}p<0.01$. D: Averages of total cell numbers in the tracks show decreasing track infiltration in the end stage tumors. N=3 tumors per conditions, student t-test, $^{**}p<0.01$. E, F: Percentage of F4/80+ macrophages that are present in the tracks of early and end stage tumors (N=3 tumors, (student t-test, $^{***}p<0.005$)) **(E)**, and percentage of F4/80+ cells in the nests (N=3 tumors, (student t-test, n. s. p=0.054)) (F). G, H: Percentage of CD206+ macrophages in the tracks (N=3 tumors, (student t-test, n.s. p=0.66)) (G), or nests (N=3 tumors, (student t-test, n.s. p=0.30)) in early and end stage tumors (H). I: Quantification of CD8+ cells in the tracks and nests of early and end stage tumors upon tissue staining as percentage of total number of dapi+ cells per field (N=5 tumors per condition). Mean ± SEM; Multiple Mann−Whitney test; * represent significant differences in the percentage of CD8+ cells in the tracks. J: Quantification of CD8+ cells in the tracks and nests of early and end stage tumors upon tissue staining expressed as relative ratio (N=5 tumors per condition). Mean ± SEM; Multiple Mann−Whitney test; * represent significant differences in the relative abundance of CD8+ cells in the nests.

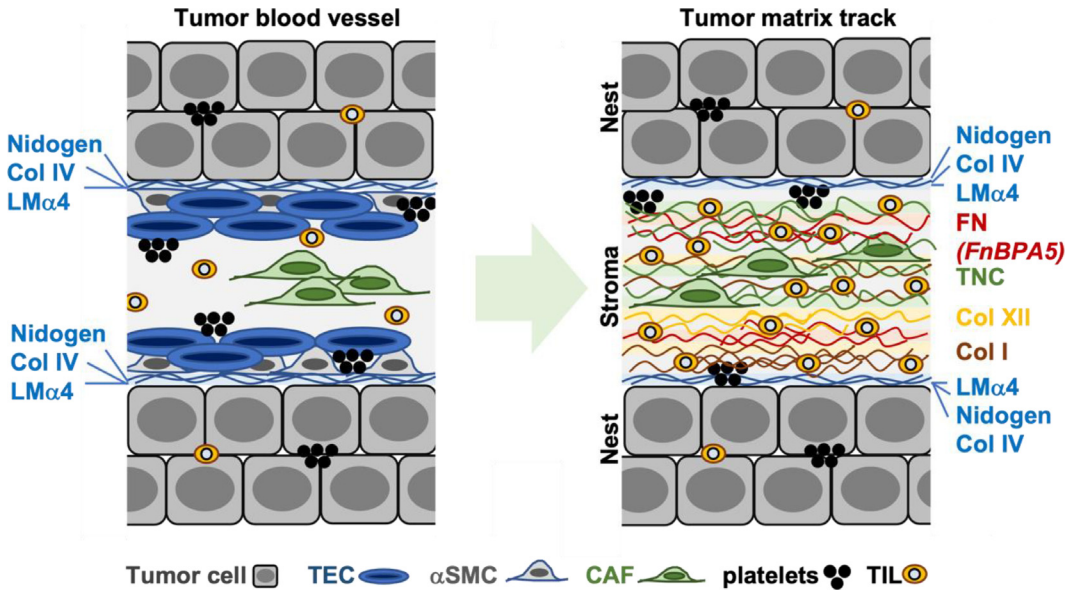

Fig. 9. Proposed model how the tumor matrix tracks could evolve from tumor blood vessels. (I) Tumor cells are separated from smooth muscle cells lining the vessel and ECs by an endothelial basement membrane composed of LMα4, ColIV and nidogen (detected by IF staining) and other ECM molecules. ECs can proliferate and create TEC clusters. Tumor vessels are leaky as platelets, and FBG are found outside the tumor vessel. (II) Several intermediate states between tumor vessel and matrix tracks may exist leading to an organization of the tumor into tumor nests separated by stroma. The matrix tracks are still lined by the blood vessel basement membrane that is connected with matrix track ECM molecules such as FN, collagens I and XII and TNC. Fibroblasts inside the tracks express ECM and soluble factors thus generating an immune suppressive niche that retains TIL, in particular macrophages and CD8 T cells.

fold (Fig. 8I). As TNC was shown to have an impact on CD8+ TIL matrix retention [7], we now compared CD8+ T cell abundance between WT/shC and KO/shTNC tumors. We noticed that the relative abundance of CD8+ T cells was over three-fold higher in WT/shC compared to KO/shTNC tumors at 3 weeks. This effect was also seen in the end stage tumors but was less prominent (Fig. 8I). By using a representation focusing on the relative distributions between nests and track (and neglecting the overall differences in numbers between time points and genotypes) a clear difference is apparent. Whereas the relative track to nest distribution between TNC high and TNC low tumors is not different at 3 weeks, a major change is seen at 11 weeks (Fig. 8J). Whilst 20% of CD8+ T cells are found in the nests of WT/shC tumors at 11 weeks, it is almost 50% infiltrating the tumor nests in the KO/shTNC tumors (Fig. 8J). These results confirm a previously published influence of TNC on CD8+ TIL retention in this model [7], but goes beyond by revealing that this retention effect is less pronounced at 3 weeks. Thus, the matrix tracks and TNC may have distinct effects on tumor immunity at different time points. Matrix tracks do not seem to impair CD8+ TIL function at 3 weeks as numbers are high. However, with time, CD8+ TIL numbers drop dramatically, while CD8+ TIL matrix retention increases thereby impairing CD8+ TIL function in the end stage tumors. More work is required to understand how track maturation contributes to TIL matrix retention and function and what roles TNC and Fn, particularly Fn fiber tension, might play as Fn fiber tension is known to regulate the affinity of Fn's molecular binding partners [42].

Altogether, our results suggest a blood vessel origin of the matrix tracks, where TNC shapes matrix track maturation and function in stromal retention of CD8+ T cells that can be assessed with the Fn fiber tension probe FnBPA5 (Fig. 9).

Discussion

Matrix tracks observed in tumor tissues that form as the tumors grow are prone to play an important role in tumor growth and progression by providing a unique environmental niche. Understanding how these tracks form and evolve is thus critical in further elucidating their roles in tumors, in finding new approaches to inhibit their formation, or in therapeutically targeting the track-entrapped cells. Upon the onset of pathogenic transformations, many once tightly-regulated processes and signaling pathways become aberrantly active [68]. Tumor cells require oxygen and nutrients to proliferate, and several mechanisms are put into place to promote tumor

growth. Among them, angiogenesis, which is triggered by the angiogenic switch and results in new vessels that provide the tumor with the required oxygen and nutrients to sustain tumor growth [18]. Additionally, low oxygen and hypoxia conditions, or even the accumulation of reactive oxygen species, are known to trigger transformation of ECM architecture and composition, that in turn promotes tumor expansion and tumor cell migration [69].

Tumor matrix tracks, rich in ECM molecules, are a manifestation of tumorigenesis in tissues, yet their origin is still debated, and we here collected indications that might give hints toward the tracks' origin by studying track composition and structure over time, in the presence and absence of TNC. Our results show that tracks have a branched architecture and that their interior is rich in parallel aligned ECM proteins such as TNC, cellular Fn, collagen I, collagen XII and dense SHG-detected collagen fiber bundles, with a primary orientation along the track axis as also seen by EM imaging. The tracks also contain many cells, such as fibroblasts, TECs, mesenchymal cells, and immune cells. We here discovered that the tracks are demarcated towards the tumor cell nests by an endothelial-like basement membrane (rich in LMα4, collagen IV and nidogen), which, together with the detection of TECs, platelets and fibrinogen associated with the tracks, are reminiscent of blood vessels and strongly point towards a blood vessel origin of the tracks.

All of our observations made here and previously [2,6,7] indicate that the following hypothesized steps could be relevant for the formation of tumor matrix tracks that likely originated from blood vessels. The presence of an endothelial basement membrane demarcating the matrix tracks supports the blood vessel origin of the tracks. As seen by FBG localization and by abundant platelet detection in the tracks, tumor blood vessels at the origin of the tracks are leaky. At this early stage, TNC and collagen XII are already lining the tumor blood vessels where they form overlapping fibrillar track-like networks. At the tumor rim, we observed TECs clusters that are enriched by collagen XII indicating a loss of normal EC identity. CD45 positive leukocytes and platelets are also enriched around these TECs. Leukocytes, expressing inflammatory cytokines and platelets, rich in TGF-β and other plasticity inducing factors may contribute to TEC expansion and EC identity loss, potentially involving EndoMT [36,70]. In support of this possibility, many plasticity regulating transcription factors are more expressed in tumors with high TNC levels, and the well-documented rise of tumorigenic factors, such as hypoxia [71] or elevated TGF-β concentrations [59,72], can in turn activate Wnt [73] and Notch [74] signaling, leading to EMT and EndoMT [35,36]. Moreover, a role of TNC in promoting EMT through TGF-β was previously described in this model [2]. A loss of EC identity may enforce vessel leakiness and hypoxia further favoring expression of plasticity-promoting molecules. Changes in cell phenotypes, likely affecting tumor cells, TECs and maybe other cells, may lead to changes in gene expression and induction of ECM such as Fn, collagen XII and TNC that accumulate inside the lumen of the vessel. Here, also fibroblasts and platelets may contribute to matrix production [75]. Eventually the reorganized and dysfunctional blood vessels develop into EC-denuded tracks as our stainings revealed. Comparison of the matrisome and an angiogenesis-associated signature of tumors with high TNC (WT/shC) and low TNC (KO/shTNC) supports the possibility of a blood vessel origin of the tracks and for matrix remodeling during track maturation. In particular, expression of pro-angiogenic factors and matrix remodeling molecules lag behind in tumors with low TNC. Our RNA seq data may allow to identify factors that are involved in the early phase of track formation, which could be further exploited to prevent transition of blood vessels into matrix tracks. Indeed, TGF-β and other plasticity driving factors could be important. In this context the newly discovered TNC targeting nanobodies and MAREMO peptides could be relevant as they impair important functions of TNC in cell adhesion, TIL matrix retention, matrix expression and matrix assembly most importantly, involving inhibition of TGF-β signaling [3,76].

The potential vessel origin of the tracks could have an impact on anti-angiogenic tumor targeting, including therapies that aim at destroying the endothelial cells. Often, this leads to escape mechanisms including EndoMT, vessel co-option and phenomena like vasculogenic mimicry amongst others [14,15,23,77]. More importantly, upon destruction of the endothelial cells, the vessel basement membrane is still present [78] and could participate not only in revascularization as previously seen, but potentially also in the formation of the described tracks subsequently promoting immune suppression previously assigned to these tracks [5–7]. Even though vessel co-option might be involved in track formation in human tissue [23] followed by an EndoMT, we consider vessel co-option as unlikely in our seeded and fast growing mouse tumor models.

Tracks mature over time which is reflected by a specific matrisome signature, significant ECM remodeling, and the infiltration of immune cells. In WT/shC tumors, tracks are present in early stage tumors (25 μm) and mature with time as indicated by a reduction in diameter in the end stage (11 weeks) tumors (15 μm), similar as observed for WT/shTNC tumors, in which the TNC is solely produced by host stromal cells. In contrast, in tumors without host-derived TNC (KO/shC), expressing very little TNC or no TNC at all, track maturation is delayed which is mirrored by specific matrisome signatures. Moreover, tracks still form even in the total absence

of TNC as seen in NeuNT-/- and other tumors as e.g. tongue tumors and PNET insulinoma [6,27]. All these observations reveal that, while TNC is not necessary to initiate track formation, its presence however does impact track maturation that is observed here between early and end tumor stages. As the tissue surrounding the tracks is rich in stroma and cancer cells, this could suggest that the uncontrolled cell division, as upregulated in the presence of TNC, builds up solid stress in the surrounding tissue, which in turn leads to squeezing of the tracks, however, only in the presence and not in the absence of TNC, similarly to the blood and lymphatic vessels collapse previously reported in advanced tumors [79,80]. Matrix remodeling might also play a role in track maturation and is altered and delayed in the absence of stromal TNC as our RNA seq data suggest, thus leading to niches with potentially different phenotypes. These properties could be important in context of immune cell infiltration and retention of tumor infiltrating CD8+ T cells, macrophages and other TIL in the tracks. Indeed, we observed more CD8+ TIL retention in 3 weeks than 11 weeks tumors. Moreover, more CD8 TIL infiltrated the tumor nests in the end stage tumors in the absence of TNC. Future studies will have to determine whether the proteoforms of tumor cell-derived and host-derived TNC is different, potentially having different functions in track maturation.

Enrichment of the track core with TNC correlates with an enhanced presence of Fn fibers in a relaxed tensional state as detected by the enhanced binding of Cy5-FnBPA5 in the core of the tracks. Reduced binding of Cy5-FnBPA5 is observed in tracks of tumors lacking TNC, which also correlates with an observed reduced assembly of SHG-positive collagen bundles. This suggests that the presence of TNC directly or indirectly impacts the tensional state of Fn fibers and thus potentially the functional display of its binding sites [42]. The comparison of gene expression profiles of tumors with high and no/low TNC revealed that TNC regulates expression of many matrix molecules, ECM crosslinking molecules such as LOX and LOXL4, and several TGF-β pathway members, suggesting a potential role of this essential pathway, that regulates mechanotransduction of cell contractility [81], in track maturation. Indeed, in comparison to TNC-low tumors, TNC-high tumors express more matrix molecules as well as more ECM degrading proteases, including MMPs-1, -2, -3, -7, -13 and -14 known to cleave Fn fibers [82,83]. TNC was shown to reduce cell adhesion through downregulation of RhoA and other pathways [64,84,85], and reduced RhoA activation is known to reduce Fn fiber tension [86]. The reduced tension of Fn fibers in the tracks could hence either be due to the TNC-induced downregulated cell contractility and reduced RhoA signaling [27,85], the upregulated expression of MMPs which could cause proteolytic Fn fiber cleavage, or the TNC-induced upregulated collagen fibrillogenesis in the tracks which then serves the contracting cells as force-bearing elements [87]. Finally, the newly assembled ECM inside the tubular structures, may attract other cells (tumor cells, fibroblasts and leukocytes [5,7]) to infiltrate from the surrounding tissue likely building up more interstitial pressure in the nascent tracks.

While it was previously shown that TNC inside of the tracks retains CD8+ T lymphocytes [7], macrophages [5] and CD11c+ myeloid cells [6], here we confirmed the presence of CD8+ T cells and macrophages (especially F480+ and CD206+macrophages) in the tracks. Importantly though, we discovered here that track maturation impacts abundance of these leukocytes inside the tumor tracks. Our data highlight the essential role of the tumor-associated tracks to retain the leukocytes at significantly higher numbers as in the surrounding tumor tissue, which is highly significant as the microenvironmental niche shaped by the track geometry and ECM will thus influence their phenotypes. Previous studies showed that macrophage confinement by adhesive micropatterned Fn stripes stabilizes the M2 phenotype in cell culture [88,89], and we here would like to propose that the prevailing M2 phenotype (CD206+) found inside the track core gets stabilized by the uniaxial geometrical confinement in the track. Furthermore, the increased expression of transcription factors ZEB1 and ZEB2 in WT versus TNC KO/KD tumors is notable, as ZEB2 is required to maintain the tissue-specific identities of macrophages [90]. As the tumor grows and the tracks mature while getting thinner, less macrophages and CD8+ T cells are found in the tumors. What happens to these infiltrating leukocytes during track maturation has to be addressed in the future but may harbor information that could be used to enforce release of CD8+ T cells and macrophages from the matrix. Additionally, recent work showed an important role of macrophages in the formation of TNC-rich niches in the metastatic lung, highlighting the importance of the EC/macrophage crosstalk in this process, and identified tumor cell-derived TNC as an important regulator of this crosstalk [91]. Interestingly, targeting VEGFA signaling did not impair this crosstalk, nor was the depletion of macrophages sufficient to prevent the formation of these pro-metastatic niches [91]. It is intriguing to speculate that the highly abundant macrophages in our tumor models have played a similar role as in the pulmonary tumor niche. Since so much is still unknown about cancer-associated niches (in the primary tumor and metastasis), our results are of prime importance as they shed light on how TNC, and perhaps even the accumulation of structurally relaxed Fn fibers, regulate and shape the evolution of these niches.

To advance immune oncology strategies to fight cancer, our finding of the retention of CD8+ T lymphocytes and macrophages (F480+, CD206+) in the tracks is remarkable: entrapment in the tracks spatially separates the immune cells from the cancer cell nests that surround the tracks and thus limits their ability to get activated through immunological synapse formation. The immune suppressive function of the tracks has been documented already earlier [7]. However, a role of Fn has not yet been addressed. Here, we describe that TNC-rich tracks retaining CD8+ T cells and macrophages also contain low tension Fn fibers. Taken together with the previous discovery that Fn fibers under low tension have a reduced binding capability for interleukin-7 (Il-7) [92], a cytokine that plays an important role in promoting T and B cells maturation and proliferation, our discovery that the tracks are filled with low-tension Fn fibers in tracks further supports that the tracks present immune modulating and immune suppressive niches for infiltrating CD8+ T cells and macrophages, that can be specifically detected using the FnBPA5 tension probe.

Materials and methods

Genetic and grafted breast tumor models

MMTV-NeuNT female mice in FVB/NCrl in a TNC KO background (described by Sun et al. [2]) were used according to the guidelines of INSERM and the ethical committee of Alsace, France (CREMEAS) (Directive 2010/63/EU on the protection of animals used for scientific purposes). TNC KO (TNC -/-) of this MMTV-NeuNT breast tumor model was obtained by serial consecutive breeding between heterozygous TNC +/- counterparts [2]. In the orthotopic syngeneic NT193 model, FVB mice with WT or TNCKO genotypes were grafted with 1×10^7 NT193 cells [46] in the surgically opened left fourth mammary gland as previously described [2]. Tumor cells (shC or TNC knockdown (sh1TNC, sh2TNC)) were engrafted into a female WT or TNCKO FVB host and arising tumors were investigated at different time points as previously described [7]. Grafting of shC tumor cells into a WT host and sh2TNC cells (referred to here as "shTNC") into a TNCKO host gave rise to TNC+ (WT/shC) and TNC- (KO/shTNC) tumors, respectively. Either 3 weeks or 11 weeks after grafting (for the NT193 model) or after 4−5 months after initial tumor palpation for the MMTV-NeuNT model, tumor-bearing mice were euthanized and breast tumors were processed for subsequent analyses: freezing in liquid nitrogen for mRNA analysis or embedding in O.C.T (Sakura Finetek) for immunostaining.

Grafted breast tumor model with different cellular sources of TNC

WT/shTNC and KO/shC breast tumor models with respectively stromal versus tumoral cellular source of TNC have been generated as described [2,5,7] (Supplementary Fig. S1C). Female FVB mice, either WT or TNCKO, were grafted with 1×10^7 NT193 cells (control (shC) or TNC knock-down (sh1TNC, sh2TNC) [2]) in the surgically opened left fourth mammary gland [2,7]. Either 3 weeks or 11 weeks after grafting, tumor-bearing mice were euthanized and breast tumors were processed for subsequent analyses: freezing in liquid nitrogen for mRNA analysis or embedding in O.C.T (Sakura Finetek) for immunostaining. All animal experiments were realized in accordance with the guidelines of INSERM and the ethical committee of Alsace, France (CREMEAS) (Directive 2010/63/EU on the protection of animals used for scientific purposes).

Gene expression analysis of the tumor models

RNA-seq data previously generated from NT193 tumors (2 replicates per condition) and NeuNT tumors (3 replicates per conditions) were used. The raw data for NT193 tumors and NeuNT tumors are available at https://www.ebi.ac.uk/arrayexpress/experiments/E-MTAB-10135 and https://www.ncbi.nlm.nih.gov/sra/?term=PRJNA587450 [5,7].

For all gene expression data, up-regulated and down-regulated genes were selected based on the p-value ($p < 0,05$) or adjusted p-value cutoff of 10% and a minimum fold-change of +/- 0.8. Gene Ontology (GO) term enrichment (GO_Biological process_2018) was performed using Enrichr tool (Ma'ayan laboratory) [93]. Deregulated gene expression analysis was performed by using the PANTHER version 11 and REACTOME software. Heatmap representation of differentially expressed genes was performed by using heatmapper website (http://www.heatmapper.ca/).

Real Time quantitative PCR analysis

Total RNA was extracted from frozen tumors with TRIzol (Invitrogen, 12044977). cDNAs (synthesized using random primers and Moloney murine leukemia virus reverse transcriptase (MultiScribe, Applied Biosystems, 10117254)) were used for qRT-PCR in an Mx3005P Real-Time PCR System (ThermoFisher Scientific) with Sybr Green Master mix (ThermoFisher Scientific, 4344463) or Fast Taqman mix (ThermoFisher Scientific, 4444557). Expression of mouse *Gapdh* mRNA (Life Technology, 433764T) was used as endogenous control in the comparative cycle threshold method (2-δδCt) with the listed primers.

Primer sequences used for qPCR		
GENE	**Forward primer**	**Reverse primer**
Twist2	TCAACCTTCTTCCCTGAAC	GATTGAGGGTGTCA ACAGA
Slug	CTCACCTCGGGAGCATACAG	GACTTACACGCCCC AAGGATG
Twist1	AGTGTTTGGCAGGGGACA	CCCATCCCCTGGGT ATCT
Zeb1	GCCAGCAGTCATGATGAAAA	TATCACAATACGGG CAGGTG
MMP14	TGGATGCCGATCAGAAGTGG	CTAGGTTGTAGATC TCCTCGT
MMP7	CTTGGATAGACTGCTCTGAG	CATTGTCCCATGCC AGATTT
MMP9	ACGACATAGACGGCATCCA	GCTGTGGTTCAGTT GTGGTG
MMP2	GGCACCTTTGAATACTCAGGA	TTTCCCAGAGACCA GAACCA
MMP3	CTGCTGGTCAGGCAGGAG	TGCCAGTTTCTTTG GCTCTT

Tumor cryosections electron microscopy imaging

Frozen and cryopreserved tissue samples were thawed up and washed with distilled water followed by a fixation in 2% (v/v) formaldehyde and 0.25% (v/v) glutaraldehyde in 100 mM cacodylate buffer, pH 7.4, at 4 °C overnight. Afterwards, tissue samples were rinsed in PBS, dehydrated in ethanol up to 70%, and embedded in LR White embedding medium (London Resin Company, UK) according to the manufacturer's instructions using UV light for polymerization. Ultrathin sections were cut with an ultramicrotome, collected on copper grids, and negatively stained with 2% uranyl acetate for 15 min. Electron micrographs were taken at 60 kV with a Philips EM-410 electron microscope using imaging plates (Ditabis, Pforzheim, Germany).

Tumor cryosections immunohistochemistry

10 μm thick tumor cryosections were thawed and rehydrated in PBS before fixation with 4% PFA for 10 min. The tissue sections were then blocked for 1 h at RT with 5% Goat Serum (G9023, Sigma) with 0.3 M glycine and further exposed to primary antibodies solution overnight at 4 °C (Supplementary Table T1). After overnight incubation with primary antibodies, followed a 1 h incubation with secondary antibodies diluted in blocking buffer solution (Supplementary Table T1). Optional DAPI stain (2 μg/ml) was realized in the last 10 min of the secondary antibody incubation and the slides were further mounted and sealed with fluorescence mounting medium (Dako, Denmark).

Cryosection staining with Cy5-FnBPA5

For Cy5-FnBPA5 staining, the Cy5-FnBPA5 tension probe was presented to the tissue sections before tissue fixation. Cryosections were thawed, rehydrated, and blocked for 30 min with 4% BSA at RT followed by incubation with 5 μg/ml of Cy5-FnBPA5, for 1 h at RT and protected from light. After 1 h, the cryosections were washed in PBS and further fixed for 10 min with 4% PFA. Subsequently, staining protocols as described above for other markers of interest were used.

Fluorescence and SHG imaging of stained tissue sections and SHG

Full tissue overview of stained cryosections of tumor tissue were imaged with a slide scanner (Panoramic 250, 3D Histec) and zoomed-in images of discrete areas of the tissue sections were acquired with a confocal microscope (Olympus FV2000 microscope). Stained cryosections of tumor tissues, with differential TNC cellular source, were imaged with a Leica SP8 confocal microscope. Full tissue overviews were acquired with a 10x air objective and tiling of multiple single area, and higher resolution images were acquired with 25x objective. SHG signal was acquired with a Leica SP8 multiphoton microscope with an excitation at λ=880 nm. WT/shC tumors immunostained with antibodies against immune cells were acquired with a fluorescence Zeiss Axio Imager Z2 microscope.

Image analysis

Confocal images were further visualized and analyzed with Fiji (ImageJ) and Matlab (Mathworks, Switzerland) as described below.

Line profile plots

Line profile plots of single track cross-sections were realized using Fiji built in "plot profile" function on selected track cross-sections, and measured data points were then transferred to Prism GraphPad where the line profile plots were plotted.

Track density analysis

For each image studied, the track density corresponds to the percentage of total tissue area covered by ECM tracks. LM and Fn signals being stable in the tracks through the conditions, tracks were defined by the combined LM and Fn channels. The tracks (LM and Fn channels together) were thresholded with Fiji built-in thresholding function. The number of pixels in the tracks correspond to the pixels whose intensity in the Fn and LM channels is superior to the threshold. Hence defined track pixels were then counted with a custom-made Matlab script and expressed as a percentage of all the pixels in the tissues (for analysis of full tissue overview) or as a percentage of all pixels in each zoom-in

image (for zoom-in images acquired with higher resolution).

Colocalization and proximity analysis

Zoom-in confocal images were first opened in Fiji, where the TNC and Cy5-FnBPA5 channels were thresholded with the respective Otsu and Yen Fiji built-in thresholding functions. Custom-made Matlab scripts were then run on the thresholded images. The Matlab scripts, in a first time, calculated the percentage of pixels per zoomed-in area represented by TNC positive pixels above a threshold. For each of these positive TNC pixels, the script then analyzed whether the corresponding pixel in the Cy5-FnBPA5 channel was also positive and above a threshold (colocalization) and whether one or more pixels positive for Cy5-FnBPA5 pixels was detected within a 3-by-3 pixels evaluation matrix surrounding this pixel position (proximity analysis). The proximity analysis was adapted from Fonta et al. [24] and, for each TNC pixel positive and above the set threshold, if at least one pixel in the 3-by-3 pixels evaluation matrix is positive in the Cy5-FnBPA5 channel, then the evaluated pixel in the TNC channel is considered proximal to Cy5-FnBPA5. Colocalized and proximal pixels are expressed as percentage of all the studied pixels above a threshold for each channel.

Immune cell quantification in the tracks

Zoom-in fluorescent images obtained with a fluorescence Zeiss Axio Imager Z2 microscope were first opened in Fiji, where a mask of the tracks was realized with the combined thresholded channels of TNC signal and Cy5-FnBPA5 signal. Cells positive for the immune markers as well as total cells stained with DAPI were counted with the built-in Analyze particles plug-in. The track mask was further applied to the channels of immune cells and DAPI and the corresponding number of cells in the tracks were obtained with the built-in Analyze particles plug-in. Cell numbers obtained were exported in a .csv file and averages of cells expressing a given marker in the tracks were further calculated in Excel from the calculated cell numbers obtained.

Statistical analysis

For proximity analysis and colocalization analysis, as well as for track diameter analysis between different tumor conditions, statistical significance between different tumor conditions was measured with a 1-way ANOVA, with a Tukey correction and significance was assessed for $*p<0.05$, $**p<0.01$, $***p<0.001$, $****p<0.0001$.

For Nidogen, Fn, Col IV and Col XII signal quantification in analyzed images, statistical significance between WT/shC and KO/shTNC tumors was calculated using Mann Whitney test and significance was assessed for $*p<0.05$, $**p<0.01$, $***p<0.001$.

For immune cell quantification in the tracks, statistical significance between early and late tumor stages was calculated with unpaired student t-test, two-tailed and significance was assessed for $*p<0.05$, $**p<0.01$, $***p<0.001$, $****p<0.0001$.

For the quantification of the ratio of CD8+ cell per field and the relative abundance of CD8+ cells, statistical significance between the different tumors and tumor stages was calculated using Multiple Mann-Whitney test and significance was assessed for $*p<0.05$, $**p<0.01$, $***p<0.001$.

Data Availability

The data that has been used is confidential.

CRediT authorship contribution statement

Charlotte M. Fonta: Data curation, Conceptualization, Formal analysis, Investigation, Visualization, Writing - original draft, Writing - review & editing. **ThomasLoustau:** Visualization, Data curation, Formal analysis, Investigation, Methodology, Writing - original draft, Writing - review & editing. **Chengbei Li:** Visualization, Data curation, Investigation. **Suchithra Poilil Surendran:** Visualization, Formal analysis, Data curation. **Uwe Hansen:** Data curation, Investigation. **Devadarssen Murdamoothoo:** Resources. **Mario C. Benn:** Writing - review & editing, Conceptualization, Formal analysis. **Ines Velazquez-Quesada:** Resources. **Raphael Carapito:** Data curation, Resources. **Gertraud Orend:** Conceptualization, Funding acquisition, Project administration, Supervision, Writing - original draft, Writing - review & editing. **Viola Vogel:** Writing - review & editing, Conceptualization, Formal analysis, Writing - original draft.

Acknowledgments

The authors thank Ellen van Obberghen-Schilling for helpful scientific discussions on tenascin-C and tumor ECM, as well as Alev Yilmaz, Fanny Steinbach, Chérine Abou Fayçal and Chantel Spencer for technical support. The authors thank the scopeM imaging facility of ETH Zurich.

Funding

This research was supported by ETH Zurich, the Swiss National Science Foundation (SNF Grant CR

32I3_156931 (VV), SNF-ANR Grant 310030E-164284/ECMpact (VV, GO), SNF Grant 31003A-175839 (VV), INCa plbio TENMAX (GO), Ligue contre le Cancer CCIRGE (GO) and Aviesan ITMO Cancer Radio 3R (GO).

Supplementary materials

Supplementary material associated with this article can be found in the online version at doi:10.1016/j.matbio.2023.01.002.

Received 11 May 2022;
Received in revised form 31 December 2022;
Accepted 12 January 2023
Available online 18 January 2023

Keywords:
Cancer;
Tumor matrix tracks;
Tenascin-C;
Fibronectin binding peptide FnBPA5;
CD8+ T cells;
M2 macrophages;
Endothelial-mesenchymal transition (EndoMT)

References

[1] C. Spenlé, I. Gasser, F. Saupe, K.P. Janssen, C. Arnold, A. Klein, M. Van Der Heyden, J. Mutterer, A. Neuville-Méchine, M.P. Chenard, D. Guenot, I. Esposito, J. Slotta-Huspenina, N. Ambartsumian, P. Simon-Assmann, G. Orend, Spatial organization of the tenascin-C microenvironment in experimental and human cancer, Cell Adhes. Migr. 9 (2015) 4–13, doi: 10.1080/19336918.2015.1005452.

[2] Z. Sun, I. Velázquez-Quesada, D. Murdamoothoo, C. Ahowesso, A. Yilmaz, C. Spenlé, G. Averous, W. Erne, F. Oberndorfer, A. Oszwald, R. Kain, C. Bourdon, P. Mangin, C. Deligne, K.S. Midwood, C. Abou-Faycal, O. Lefebvre, A. Klein, M. van der Heyden, M.-P. Chenard, G. Christofori, C. Mathelin, T. Loustau, T. Hussenet, G. Orend, Tenascin-C Increases Lung Metastasis by Impacting Blood Vessel Invasions, Elsevier, 2019, doi: 10.1016/J.MATBIO.2019.07.001.

[3] A. Yilmaz, T. Loustau, N.S. Salomé1, S.P. Surendran, C. Li, R.P. Tucker, V. Izzi, R. Lamba, M. Koch, G. Orend, Advances on the roles of Tenascin-C in cancer, J. Cell Sci. 135 (2022), doi: 10.1242/JCS.260244.

[4] E. Kääriäinen, P. Nummela, J. Soikkeli, M. Yin, M. Lukk, T. Jahkola, S. Virolainen, A. Ora, E. Ukkonen, O. Saksela, E. Hölttä, Switch to an invasive growth phase in melanoma is associated with Tenascin-C, fibronectin, and Procollagen-I forming specific channel structures for invasion, J. Pathol. 210 (2006) 181–191, doi: 10.1002/path.2045.

[5] C. Deligne, D. Murdamoothoo, A.N. Gammage, M. Gschwandtner, W. Erne, T. Loustau, A.M. Marzeda, R. Carapito, N. Paul, I. Velazquez-Quesada, I. Mazzier, Z. Sun, G. Orend, K.S. Midwood, Matrix-targeting immunotherapy controls tumor growth and spread by switching macrophage phenotype, Cancer Immunol. Res. 8 (2020) 368–382, doi: 10.1158/2326-6066.CIR-19-0276.

[6] C. Spenle, T. Loustau, D. Murdamoothoo, W. Erne, S. Beghelli-De la Forest Divonne, R. Veber, L. Petti, P. Bourdely, M. Morgelin, E.M. Brauchle, G. Cremel, V. Randrianarisoa, A. Camara, S. Rekima, S. Schaub, K. Nouhen, T. Imhof, U. Hansen, N. Paul, R. Carapito, N. Pythoud, A. Hirschler, C. Carapito, H. ene Dumortier, C.G. Mueller, M. Koch, K. Schenke-Layland, S. Kon, A. Sudaka, F. Anjuere, E. van Obberghen-Schilling, G. Orend, Tenascin-C orchestrates an immune-suppressive tumor microenvironment in oral squamous cell carcinoma, Cancer Immunol. Res. 8 (2020) 1122–1138, doi: 10.1158/2326-6066.CIR-20-0074.

[7] D. Murdamoothoo, Z. Sun, A. Yilmaz, G. Riegel, C. Abou-Faycal, C. Deligne, I. Velazquez-Quesada, W. Erne, M. Nascimento, M. Mörgelin, G. Cremel, N. Paul, R. Carapito, R. Veber, H. Dumortier, J. Yuan, K.S. Midwood, T. Loustau, G. Orend, Tenascin-C immobilizes infiltrating T lymphocytes through CXCL12 promoting breast cancer progression, EMBO Mol. Med. (2021), doi: 10.15252/emmm.202013270.

[8] L.A. Tomko, R.C. Hill, A. Barrett, J.M. Szulczewski, M.W. Conklin, K.W. Eliceiri, P.J. Keely, K.C. Hansen, S.M. Ponik, Targeted matrisome analysis identifies Thrombospondin-2 and Tenascin-C in aligned collagen stroma from invasive breast carcinoma, Sci. Rep. 8 (2018) 1–11, doi: 10.1038/s41598-018-31126-w.

[9] M.W. Conklin, J.C. Eickhoff, K.M. Riching, C.A. Pehlke, K.W. Eliceiri, P.P. Provenzano, A. Friedl, P.J. Keely, Aligned collagen is a prognostic signature for survival in human breast carcinoma, Am J Pathol. 178 (2011) 1221–1232, doi: 10.1016/j.ajpath.2010.11.076.

[10] J.E. Gretz, E.P. Kaldjian, A.O. Anderson, S. Shaw, Sophisticated strategies for information encounter in the lymph node: the reticular network as a conduit of soluble information and a highway for cell traffic, J. Immunol. 157 (1996) 495–499 http://www.ncbi.nlm.nih.gov/pubmed/8752893 accessed January 23, 2020.

[11] M. Sixt, N. Kanazawa, M. Selg, T. Samson, G. Roos, D.P. Reinhardt, R. Pabst, M.B. Lutz, L. Sorokin, The conduit system transports soluble antigens from the afferent lymph to resident dendritic cells in the T cell area of the lymph node, Immunity 22 (2005) 19–29, doi: 10.1016/j.immuni.2004.11.013.

[12] M. Drumea-Mirancea, J.T. Wessels, C.A. Müller, M. Essl, J.A. Eble, E. Tolosa, M. Koch, D.P. Reinhardt, M. Sixt, L. Sorokin, Y.D. Stierhof, H. Schwarz, G. Klein, Characterization of a conduit system containing laminin-5 in the human thymus: a potential transport system for small molecules, J. Cell Sci. 119 (2006) 1396–1405, doi: 10.1242/jcs.02840.

[13] M. Papanicolaou, A.L. Parker, M. Yam, E.C. Filipe, S.Z. Wu, J.L. Chitty, K. Wyllie, E. Tran, E. Mok, A. Nadalini, J.N. Skhinas, M.C. Lucas, D. Herrmann, M. Nobis, B.A. Pereira, A.M.K. Law, L. Castillo, K.J. Murphy, A. Zaratzian, J.F. Hastings, D.R. Croucher, E. Lim, B.G. Oliver, F.V. Mora, B.L. Parker, D. Gallego-Ortega, A. Swarbrick, S. O'Toole, P. Timpson, T.R. Cox,

Temporal profiling of the breast tumour microenvironment reveals collagen XII as a driver of metastasis, Nat. Commun. 131 (13) (2022) 1–21 2022, doi: 10.1038/s41467-022-32255-7.

[14] A.J. Maniotis, R. Folberg, A. Hess, E.A. Seftor, L.M.G. Gardner, J. Pe'er, J.M. Trent, P.S. Meltzer, M.J.C. Hendrix, Vascular channel formation by human melanoma cells *in vivo* and *in vitro*: vasculogenic mimicry, Am. J. Pathol. 155 (1999) 739–752, doi: 10.1016/S0002-9440(10)65173-5.

[15] R. Folberg, A.J. Maniotis, Vasculogenic mimicry, APMIS 112 (2004) 508–525, doi: 10.1111/j.1600-0463.2004.apm11207-0810.x.

[16] Z. Lokmic, T. Lämmermann, M. Sixt, S. Cardell, R. Hallmann, L. Sorokin, The extracellular matrix of the spleen as a potential organizer of immune cell compartments, Semin. Immunol. 20 (2008) 4–13, doi: 10.1016/J.SMIM.2007.12.009.

[17] F.B. Kai, A.P. Drain, V.M. Weaver, The extracellular matrix modulates the metastatic journey, Dev. Cell. 49 (2019) 332–346, doi: 10.1016/j.devcel.2019.03.026.

[18] B. Langlois, F. Saupe, T. Rupp, C. Arnold, M. Van der Heyden, G. Orend, T. Hussenet, AngioMatrix, a signature of the tumor angiogenic switch-specific matrisome, correlates with poor prognosis for glioma and colorectal cancer patients, Oncotarget 5 (2014) 10529–10545, doi: 10.18632/oncotarget.2470.

[19] J. Folkman, K. Watson, D. Hanahan, Induction of angiogenesis during the transition from hyperplasia to neoplasia, Nature 339 (1989) 58–61.

[20] D. Hanahan, J. Folkman, Patterns and emerging mechanisms of the angiogenic switch during tumorigenesis, Cell 86 (1996) 353–364, doi: 10.1016/S0092-8674(00)80108-7.

[21] D. Ribatti, B. Nico, E. Crivellato, A.M. Roccaro, A. Vacca, The history of the angiogenic switch concept, Leukemia 21 (2007) 44–52, doi: 10.1038/sj.leu.2404402.

[22] G. Bergers, L.E. Benjamin, Tumorigenesis and the angiogenic switch, Nat. Rev. Cancer. 3 (2003) 401–410, doi: 10.1038/nrc1093.

[23] E.A. Kuczynski, P.B. Vermeulen, F. Pezzella, R.S. Kerbel, A.R. Reynolds, Vessel co-option in cancer, Nat. Rev. Clin. Oncol. 168 (16) (2019) 469–493 2019, doi: 10.1038/s41571-019-0181-9.

[24] C.M. Fonta, S. Arnoldini, D. Jaramillo, A. Moscaroli, A. Oxenius, M. Behe, V. Vogel, Fibronectin fibers are highly tensed in healthy organs in contrast to tumors and virus-infected lymph nodes, Matrix Biol. Plus. 8 (2020), doi: 10.1016/j.mbplus.2020.100046.

[25] K.S. Midwood, M. Chiquet, R.P. Tucker, G. Orend, Tenascin-C at a glance, J. Cell Sci. 129 (2016) 4321–4327, doi: 10.1242/jcs.190546.

[26] K. Midwood, S. Sacre, A.M. Piccinini, J. Inglis, A. Trebaul, E. Chan, S. Drexler, N. Sofat, M. Kashiwagi, G. Orend, F. Brennan, B. Foxwell, Tenascin-C is an endogenous activator of Toll-like receptor 4 that is essential for maintaining inflammation in arthritic joint disease, Nat. Med. 157 (15) (2009) 774–780 2009, doi: 10.1038/nm.1987.

[27] F. Saupe, A. Schwenzer, Y. Jia, I. Gasser, C. Spenlé, B. Langlois, M. Kammerer, O. Lefebvre, R. Hlushchuk, T. Rupp, M. Marko, M. van der Heyden, G. Cremel, C. Arnold, A. Klein, P. Simon-Assmann, V. Djonov, A. Neuville-Méchine, I. Esposito, J. Slotta-Huspenina, K.P. Janssen, O. DeWever, G. Christofori, T. Hussenet, G. Orend, Tenascin-C downregulates Wnt inhibitor dickkopf-1, promoting tumorigenesis in a neuroendocrine tumor model, Cell Rep. 5 (2013) 482–492, doi: 10.1016/j.celrep.2013.09.014.

[28] G.J. Bakker, S. Weischer, J.F. Ortas, J. Heidelin, V. Andresen, M. Beutler, E. Beaurepaire, P. Friedl, Intravital deep-tumor single-beam 3-photon, 4-photon, and harmonic microscopy, Elife 11 (2022), doi: 10.7554/ELIFE.63776.

[29] L. Zuliani-Alvarez, A.M. Marzeda, C. Deligne, A. Schwenzer, F.E. McCann, B.D. Marsden, A.M. Piccinini, K.S. Midwood, Mapping tenascin-C interaction with toll-like receptor 4 reveals a new subset of endogenous inflammatory triggers, Nat. Commun. 8 (2017) 1–14, doi: 10.1038/s41467-017-01718-7.

[30] A. Naba, K.R. Clauser, S. Hoersch, H. Liu, S.A. Carr, R.O. Hynes, The matrisome: in silico definition and *in vivo* characterization by proteomics of normal and tumor extracellular matrices, Mol. Cell. Proteomics 11 (2012), doi: 10.1074/mcp.M111.014647.

[31] S. Schéele, A. Nyström, M. Durbeej, J.F. Talts, M. Ekblom, P. Ekblom, Laminin isoforms in development and disease, J. Mol. Med. 858 (85) (2007) 825–836 2007, doi: 10.1007/S00109-007-0182-5.

[32] P. Tunggal, N. Smyth, M. Paulsson, M.C. Ott, Laminins: structure and genetic regulation, Microsc. Res. Technol. 51 (2000) 214–227, doi: 10.1002/1097-0029.

[33] L. Nagl, L. Horvath, A. Pircher, D. Wolf, Tumor endothelial cells (TECs) as potential immune directors of the tumor microenvironment – new findings and future perspectives, Front. Cell Dev. Biol. 8 (2020) 1–18, doi: 10.3389/fcell.2020.00766.

[34] J. Goveia, K. Rohlenova, F. Taverna, L. Treps, L.C. Conradi, A. Pircher, V. Geldhof, L.P.M.H. de Rooij, J. Kalucka, L. Sokol, M. García-Caballero, Y. Zheng, J. Qian, L.A. Teuwen, S. Khan, B. Boeckx, E. Wauters, H. Decaluwé, P. De Leyn, J. Vansteenkiste, B. Weynand, X. Sagaert, E. Verbeken, A. Wolthuis, B. Topal, W. Everaert, H. Bohnenberger, A. Emmert, D. Panovska, F. De Smet, F.J.T. Staal, R.J. Mclaughlin, F. Impens, V. Lagani, S. Vinckier, M. Mazzone, L. Schoonjans, M. Dewerchin, G. Eelen, T.K. Karakach, H. Yang, J. Wang, L. Bolund, L. Lin, B. Thienpont, X. Li, D. Lambrechts, Y. Luo, P. Carmeliet, An integrated gene expression landscape profiling approach to identify lung tumor endothelial cell heterogeneity and angiogenic candidates, Cancer Cell. 37 (2020) 21–36 e13, doi: 10.1016/j.ccell.2019.12.001.

[35] S. Piera-Velazquez, F. Mendoza, S. Jimenez, Endothelial to Mesenchymal Transition (EndoMT) in the pathogenesis of human fibrotic diseases, J. Clin. Med. 5 (2016) 45, doi: 10.3390/jcm5040045.

[36] V. Platel, S. Faure, I. Corre, N. Clere, Endothelial-to-mesenchymal transition (EndoMT): roles in tumorigenesis, metastatic extravasation and therapy resistance, J. Oncol. (2019) 2019, doi: 10.1155/2019/8361945.

[37] P. Baluk, D.M. McDonald, Markers for microscopic imaging of lymphangiogenesis and angiogenesis, Ann. N. Y. Acad. Sci. (2008) 1–12 Blackwell Publishing Inc., doi: 10.1196/annals.1413.001.

[38] T. Oskarsson, S. Acharyya, X.H.F. Zhang, S. Vanharanta, S.F. Tavazoie, P.G. Morris, R.J. Downey, K. Manova-Todorova, E. Brogi, J. Massagué, Breast cancer cells produce tenascin C as a metastatic niche component to colonize the lungs, Nat. Med. 17 (2011) 867–874, doi: 10.1038/nm.2379.

[39] L. Fattet, H.Y. Jung, M.W. Matsumoto, B.E. Aubol, A. Kumar, J.A. Adams, A.C. Chen, R.L. Sah, A.J. Engler,

E.B. Pasquale, J. Yang, Matrix rigidity controls epithelial-mesenchymal plasticity and tumor metastasis *via* a mechanoresponsive EPHA2/LYN complex, Dev. Cell. 54 (2020) 302–316 e7, doi: 10.1016/j.devcel.2020.05.031.

[40] S. Arnoldini, A. Moscaroli, M. Chabria, M. Hilbert, S. Hertig, R. Schibli, M. Béhé, V. Vogel, Novel peptide probes to assess the tensional state of fibronectin fibers in cancer, Nat. Commun. 8 (2017), doi: 10.1038/s41467-017-01846-0.

[41] M. Chabria, S. Hertig, M.L. Smith, V. Vogel, Stretching fibronectin fibres disrupts binding of bacterial adhesins by physically destroying an epitope, Nat. Commun. 1 (2010), doi: 10.1038/ncomms1135.

[42] V. Vogel, Unraveling the mechanobiology of extracellular matrix, Annu. Rev. Physiol. 80 (2018) 353–387, doi: 10.1146/annurev-physiol-021317-121312.

[43] L. Bouchard, L. Lamarre, P.J. Tremblay, P. Jolicoeur, Stochastic appearance of mammary tumors in transgenic mice carrying the MMTV/c-neu oncogene, Cell 57 (1989) 931–936, doi: 10.1016/0092-8674(89)90331-0.

[44] W.J. Muller, E. Sinn, P.K. Pattengale, R. Wallace, P. Leder, Single-step induction of mammary adenocarcinoma in transgenic mice bearing the activated c-neu oncogene, Cell 54 (1988) 105–115, doi: 10.1016/0092-8674(88)90184-5.

[45] P.M. Siegel, W. Shu, R.D. Cardiff, W.J. Muller, J. Massagué, Transforming growth factor β signaling impairs Neu-induced mammary tumorigenesis while promoting pulmonary metastasis, Proc. Natl. Acad. Sci. 100 (2003) 8430–8435, doi: 10.1073/PNAS.0932636100.

[46] A. Arpel, P. Sawma, C. Spenlé, J. Fritz, L. Meyer, N. Garnier, I. Velázquez-Quesada, T. Hussenet, S. Aci-Sèche, N. Baumlin, M. Genest, D. Brasse, P. Hubert, G. Crémel, G. Orend, P. Laquerrière, D. Bagnard, Transmembrane domain targeting peptide antagonizing ErbB2/Neu inhibits breast tumor growth and metastasis, Cell Rep. 8 (2014) 1714–1721, doi: 10.1016/j.celrep.2014.07.044.

[47] J.I. Paul, J.E. Schwarzbauer, J.W. Tamkun, R.O. Hynes, Cell-type-specific fibronectin subunits generated by alternative splicing, J. Biol. Chem. 261 (1986) 12258–12265, doi: 10.1016/S0021-9258(18)67233-3.

[48] J.E. Schwarzbauer, D.W. DeSimone, Fibronectins, their fibrillogenesis, and *in vivo* functions, Cold Spring Harb. Perspect. Biol. 3 (2011) 1–19, doi: 10.1101/CSHPERSPECT.A005041.

[49] W.S. To, K.S. Midwood, Plasma and cellular fibronectin: distinct and independent functions during tissue repair, Fibrogenesis Tissue Repair 4 (2011) 21, doi: 10.1186/1755-1536-4-21.

[50] L. Alarcon-Martinez, S. Yilmaz-Ozcan, M. Yemisci, J. Schallek, K. Kılıç, A. Can, A. Di Polo, T. Dalkara, Capillary pericytes express α-smooth muscle actin, which requires prevention of filamentous-actin depolymerization for detection, Elife 7 (2018), doi: 10.7554/ELIFE.34861.

[51] C. Anderberg, S.I. Cunha, Z. Zhai, E. Cortez, E. Pardali, J.R. Johnson, M. Franco, M. Páez-Ribes, R. Cordiner, J. Fuxe, B.R. Johansson, M.J. Goumans, O. Casanovas, P. ten Dijke, H.M. Arthur, K. Pietras, Deficiency for endoglin in tumor vasculature weakens the endothelial barrier to metastatic dissemination, J. Exp. Med. 210 (2013) 563–579, doi: 10.1084/JEM.20120662.

[52] S.H. Choi, A.R. Kim, J.K. Nam, J.M. Kim, J.Y. Kim, H.R. Seo, H.J. Lee, J. Cho, Y.J. Lee, Tumour-vasculature development *via* endothelial-to-mesenchymal transition after radiotherapy controls CD44v6+ cancer cell and macrophage polarization, Nat. Commun. 91 (9) (2018) 1–18 2018, doi: 10.1038/s41467-018-07470-w.

[53] M. Chiquet, D.E. Birk, C.G. Bönnemann, M. Koch, XII Collagen, Protecting bone and muscle integrity by organizing collagen fibrils, Int. J. Biochem. Cell Biol. 53 (2014) 51–54, doi: 10.1016/j.biocel.2014.04.020.

[54] K.R. Levental, H. Yu, L. Kass, J.N. Lakins, M. Egeblad, J.T. Erler, S.F.T. Fong, K. Csiszar, A. Giaccia, W. Weninger, M. Yamauchi, D.L. Gasser, V.M. Weaver, Matrix crosslinking forces tumor progression by enhancing integrin signaling, Cell 139 (2009) 891–906, doi: 10.1016/j.cell.2009.10.027.

[55] J.T. Erler, K.L. Bennewith, T.R. Cox, G. Lang, D. Bird, A. Koong, Q.T. Le, A.J. Giaccia, Hypoxia-induced lysyl oxidase is a critical mediator of bone marrow cell recruitment to form the premetastatic niche, Cancer Cell 15 (2009) 35–44, doi: 10.1016/J.CCR.2008.11.012.

[56] H.E. Barker, T.R. Cox, J.T. Erler, The rationale for targeting the LOX family in cancer, Nat. Rev. Cancer 12 (2012) 540–552, doi: 10.1038/nrc3319.

[57] A. Leask, D.J. Abraham, TGF-β signaling and the fibrotic response, FASEB J 18 (2004) 816–827, doi: 10.1096/fj.03-1273rev.

[58] J. Massagué, TGFβ signalling in context, Nat. Rev. Mol. Cell Biol. 13 (2012) 616–630, doi: 10.1038/nrm3434.

[59] J. Massagué, TGFb in cancer, Cell 134 (2008) 215–230, doi: 10.1016/j.cell.2008.07.001.TGF.

[60] Y. Yoshimatsu, T. Watabe, Emerging roles of inflammation-mediated endothelial–mesenchymal transition in health and disease, Inflamm. Regen. 42 (2022) 1–21, doi: 10.1186/S41232-021-00186-3/TABLES/3.

[61] S. Drápela, J. Bouchal, M.K. Jolly, Z. Culig, K. Souček, ZEB1: a critical regulator of cell plasticity, DNA damage response, and therapy resistance, Front. Mol. Biosci. 7 (2020) 36, doi: 10.3389/FMOLB.2020.00036.

[62] J.C. Adams, J. Lawler, The thrombospondins, Cold Spring Harb. Perspect. Biol. 3 (2011) 1–29, doi: 10.1101/CSHPERSPECT.A009712.

[63] R. Chiquet-Ehrismann, Anti-adhesive molecules of the extracellular matrix, Curr. Opin. Cell Biol. (1991) 800–804.

[64] R. Chiquet-Ehrismann, R.P. Tucker, Tenascins and the importance of adhesion modulation, Cold Spring Harb. Perspect. Biol. 3 (2011) 1–19, doi: 10.1101/cshperspect.a004960.

[65] S. Roth, I. Freund, Optical second-harmonic scattering in rat-tail tendon, Biopolymers 20 (1981) 1271–1290, doi: 10.1002/bip.1981.360200613.

[66] G.C. Cox, F. Manconi, E. Kable, Second harmonic imaging of collagen in mammalian tissue, Proc. SPIE 4620 (2002) 148–156, doi: 10.1117/12.470689.

[67] E. Bengtsson, M. Mörgelin, T. Sasaki, R. Timpl, D. Heinegård, A. Aspberg, The leucine-rich repeat protein PRELP binds perlecan and collagens and may function as a basement membrane anchor, J. Biol. Chem. 277 (2002) 15061–15068, doi: 10.1074/JBC.M108285200.

[68] D. Hanahan, R.A. Weinberg, The hallmarks of cancer, Cell 100 (2000) 57–70, doi: 10.1007/s00262-010-0968-0.

[69] J. Winkler, A. Abisoye-Ogunniyan, K.J. Metcalf, Z. Werb, Concepts of extracellular matrix remodelling in tumour progression and metastasis, Nat. Commun. (2020) 11, doi: 10.1038/S41467-020-18794-X.

[70] M. Labelle, S. Begum, R.O. Hynes, Direct signaling between platelets and cancer cells induces an epithelial-

mesenchymal-like transition and promotes metastasis, Cancer Cell 20 (2011) 576–590, doi: 10.1016/j.ccr.2011.09.009.
[71] M. Höckel, P. Vaupel, Tumor hypoxia: definitions and current clinical, biologic, and molecular aspects, JNCI J. Natl. Cancer Inst. 93 (2001) 266–276, doi: 10.1093/JNCI/93.4.266.
[72] S.B. Jakowlew, Transforming growth factor-β in Cancer Metastasis Rev. 25 (2006) 435-57. https://doi.org/10.1007/s10555-006-9006-2.
[73] A. Akhmetshina, K. Palumbo, C. Dees, C. Bergmann, P. Venalis, P. Zerr, A. Horn, T. Kireva, C. Beyer, J. Zwerina, H. Schneider, A. Sadowski, M.O. Riener, O.A. MacDougald, O. Distler, G. Schett, J.H.W. Distler, Activation of canonical Wnt signalling is required for TGF-β-mediated fibrosis, Nat. Commun. 3 (2012) 1–12, doi: 10.1038/ncomms1734.
[74] J. Liu, F. Dong, J. Jeong, T. Masuda, C.G. Lobe, Constitutively active Notch1 signaling promotes endothelial-mesenchymal transition in a conditional transgenic mouse model, Int. J. Mol. Med. 34 (2014) 669–676, doi: 10.3892/IJMM.2014.1818.
[75] S. Lickert, M. Kenny, K. Selcuk, J.L. Mehl, M. Bender, S.M. Früh, M.A. Burkhardt, J.D. Studt, B. Nieswandt, I. Schoen, V. Vogel, Platelets drive fibronectin fibrillogenesis using integrin αIIbβ3, Sci. Adv. 8 (2022) 8331, doi: 10.1126/SCIADV.ABJ8331/SUPPL_FILE/SCIADV.ABJ8331_-MOVIE_S1.ZIP.
[76] S. Dhaouadi, R. Ben Abderrazek, T. Loustau, C. Abou-Faycal, A. Ksouri, W. Erne, D. Murdamoothoo, M. Mörgelin, A. Kungl, A. Jung, S. Ledrappier, Z. Benlasfar, S. Bichet, R. Chiquet-Ehrismann, I. Hendaoui, G. Orend, B. Bouhaouala-Zahar, Novel human Tenascin-C function-blocking camel single domain nanobodies, Front. Immunol. 12 (2021) 660, doi: 10.3389/FIMMU.2021.635166/BIBTEX.
[77] R. Folberg, M.J.C. Hendrix, A.J. Maniotis, Vasculogenic mimicry and tumor angiogenesis, Am. J. Pathol. 156 (2000) 361–381, doi: 10.1016/S0002-9440(10)64739-6.
[78] M.R. Mancuso, R. Davis, S.M. Norberg, S. O'Brien, B. Sennino, T. Nakahara, V.J. Yao, T. Inai, P. Brooks, B. Freimark, D.R. Shalinsky, D.D. Hu-Lowe, D.M. McDonald, Rapid vascular regrowth in tumors after reversal of VEGF inhibition, J. Clin. Invest. 116 (2006) 2610–2621, doi: 10.1172/JCI24612.
[79] T. Stylianopoulos, J.D. Martin, V.P. Chauhan, S.R. Jain, B. Diop-Frimpong, N. Bardeesy, B.L. Smith, C.R. Ferrone, F.J. Hornicek, Y. Boucher, L.L. Munn, R.K. Jain, Causes, consequences, and remedies for growth-induced solid stress in murine and human tumors, Proc. Natl. Acad. Sci. USA 109 (2012) 15101–15108, doi: 10.1073/PNAS.1213353109.
[80] V.P. Chauhan, Y. Boucher, C.R. Ferrone, S. Roberge, J.D. Martin, T. Stylianopoulos, N. Bardeesy, R.A. DePinho, T.P. Padera, L.L. Munn, R.K. Jain, Compression of pancreatic tumor blood vessels by hyaluronan is caused by solid stress and not interstitial fluid pressure, Cancer Cell 26 (2014) 14, doi: 10.1016/J.CCR.2014.06.003.
[81] S. Chen, M. Crawford, R.M. Day, V.R. Briones, J.E. Leader, P.A. Jose, R.J. Lechleider, RhoA modulates smad signaling during transforming growth factor-β-induced smooth muscle differentiation, J. Biol. Chem. 281 (2006) 1765–1770, doi: 10.1074/JBC.M507771200.
[82] R. Visse, H. Nagase, Matrix metalloproteinases and tissue inhibitors of metalloproteinases: structure, function, and biochemistry, Circ. Res. 92 (2003) 827–839, doi: 10.1161/01.RES.0000070112.80711.3D.
[83] X. Zhang, C.T. Chen, M. Bhargava, P.A. Torzilli, A comparative study of fibronectin cleavage by MMP-1, -3, -13, and -14, Cartilage 3 (2012) 267–277, doi: 10.1177/1947603511435273.
[84] K. Imanaka-Yoshida, H. Aoki, Tenascin-C and mechanotransduction in the development and diseases of cardiovascular system, Front. Physiol. (2014) 1–12 5 JUL, doi: 10.3389/fphys.2014.00283.
[85] M.B. Wenk, K.S. Midwood, J.E. Schwarzbauer, Tenascin-C suppresses Rho activation, J. Cell Biol. 150 (2000) 913–919, doi: 10.1083/jcb.150.4.913.
[86] G. Baneyx, L. Baugh, V. Vogel, Fibronectin extension and unfolding within cell matrix fibrils controlled by cytoskeletal tension, Proc. Natl. Acad. Sci. USA 99 (2002) 5139–5143, doi: 10.1073/pnas.072650799.
[87] K.E. Kubow, R. Vukmirovic, L. Zhe, E. Klotzsch, M.L. Smith, D. Gourdon, S. Luna, V. Vogel, Mechanical forces regulate the interactions of fibronectin and collagen I in extracellular matrix, Nat. Commun. 6 (2015), doi: 10.1038/ncomms9026.
[88] F.Y. McWhorter, T. Wang, P. Nguyen, T. Chung, W.F. Liu, Modulation of macrophage phenotype by cell shape, Proc. Natl. Acad. Sci. USA 110 (2013) 17253–17258, doi: 10.1073/PNAS.1308887110/SUPPL_FILE/PNAS.201308887SI.PDF.
[89] N. Jain, V. Vogel, Spatial confinement downsizes the inflammatory response of macrophages, Nat. Mater. 1 (2018), doi: 10.1038/s41563-018-0190-6.
[90] C.L. Scott, W. T'Jonck, L. Martens, H. Todorov, D. Sichien, B. Soen, J. Bonnardel, S. De Prijck, N. Vandamme, R. Cannoodt, W. Saelens, B. Vanneste, W. Toussaint, P. De Bleser, N. Takahashi, P. Vandenabeele, S. Henri, C. Pridans, D.A. Hume, B.N. Lambrecht, P. De Baetselier, S.W.F. Milling, J.A. Van Ginderachter, B. Malissen, G. Berx, A. Beschin, Y. Saeys, M. Guilliams, The transcription factor ZEB2 is required to maintain the tissue-specific identities of macrophages, Immunity 49 (2018) 312–325 e5, doi: 10.1016/J.IMMUNI.2018.07.004.
[91] T. Hongu, M. Pein, J. Insua-Rodríguez, E. Gutjahr, G. Mattavelli, J. Meier, K. Decker, A. Descot, M. Bozza, R. Harbottle, A. Trumpp, H.P. Sinn, A. Riedel, T. Oskarsson, Perivascular tenascin C triggers sequential activation of macrophages and endothelial cells to generate a pro-metastatic vascular niche in the lungs, Nat. Cancer 34 (3) (2022) 486–504 2022, doi: 10.1038/s43018-022-00353-6.
[92] D. Ortiz Franyuti, M. Mitsi, V. Vogel, Mechanical stretching of fibronectin fibers upregulates binding of Interleukin-7, Nano Lett. 18 (2018) 15–25, doi: 10.1021/acs.nanolett.7b01617.
[93] E.Y. Chen, C.M. Tan, Y. Kou, Q. Duan, Z. Wang, G.V. Meirelles, N.R. Clark, A. Ma'ayan, Enrichr: interactive and collaborative HTML5 gene list enrichment analysis tool, BMC Bioinf. 14 (2013) 1–14, doi: 10.1186/1471-2105-14-128/FIGURES/3.